

Responses to the Reviewer

Retrieval of the thickness of undeformed sea ice from Simulated C-band compact polarimetric SAR images

X. Zhang, and W. Dierking

Part I

To the editor and Dr. Kern:

We have revised the paper to address the main issues raised by the reviewers, as well as to include minor modifications of the authors. In the following list, we first address the major issues that are of importance in general, then we refer to the issues raised by Dr. Kern. The major revisions of this paper including 4 parts:

- (1) We reorganized Section 1 “introduction”. We emphasized the significance of retrieving the sea ice thickness distribution from CP SAR both in the ice services and sea ice forecasting. And an overview of the differences between dual-, quad- and compact-polarimetric modes was provided.
- (2) In section 3 “simulation”, we carefully discuss the effect of snow layer, and we used real scenario roughness parameters to evaluate the rough surface scattering contribution now.
- (3) For data process in Section 4.2, the processing chains were described detailed. The procedure of ice drift correction was provided. The method of segmentation level and deformed ice was modified, the new processing chain can exclude deformed ice, and the ice thickness values > 2.2 m has been passed.
- (4) The limitations (including snow layer and environment conditions) and outlook of our method was described and discussed.

Detailed response to the reviewers’ comments is below. Reviewers’ comments are in italic immediately followed by our response.

General Comments

This paper combines a thermodynamic sea ice model with a model to simulate sea ice radar backscatter to develop a new method to estimate sea ice thickness from spaceborne SAR imagery obtained at C-Band. The method is limited to level first-year ice with snow covers < 20 cm thickness during winter conditions. The method requires polarimetric observations BUT is based on a novel way to obtain the polarimetric information from compact polarization mode SAR imagery. Results of the simulations show convincing evidence that the CP-Ratio is sufficiently sensitive to the sea ice thickness - within certain bounds. Results from contemporary helicopter-borne sea ice thickness surveys and quad-polarization SAR imagery confirms the applicability of the method and illustrates that SIT can be computed from CP SAR imagery also practically.

This is a nice paper. It is easy to read. It is well structured. It touches a hot topic. It contains very interesting information and should definitely be published.

The paper would benefit from - a better introduction which better embeds and motivates

the study in the context of research dedicated to sea ice thickness retrieval in general and, in particular, from space-borne (!) SAR. - a more careful treatment of the potential limitations of the method in connection to the model simulations. - an extended interpretation and discussion of the simulation and in particular the experimental results - again in the light of the potential limitations but also in the light of the environmental conditions and the working steps done. The latter seem not to have been described detailed enough at places. - a more thorough discussion / outlook about how this promising method could be implemented practically.

In this version, we reorganized Section 1 “Introduction”, and we emphasized the importance of retrieving the sea ice thickness distribution from CP SAR in the present demand. Because of the extensive changes we made in the introduction, it is difficult to relate single parts of the modified text to the old text. The new introduction should be read in its entirety. About simulations, we carefully discuss the effect of snow layer. For simulating the rough surface scattering contribution, we now used real scenario roughness parameters. In the experimental results, we included the comparison between simulation and experimental results. Last, a discussion about limitations, outlook of our method was described.

Specific Comments

P5446, L6: What is meant by "optimal conditions"? Are these environmental conditions?
The "optimal conditions" means optimal sea ice conditions and radar parameters. Thanks, has been changed.

P5446, L7: Please specify what "CTLR" means
Thanks, has been changed to circular transmit, linear receive (CTLR) mode.

P5446, L9: "Sea of Labrador" -> "Labrador Sea" One could add "different" before "empirical".
Done.

P5446, L16-L21: You want to motivate that sea ice thickness is an important parameter to better understand the spatiotemporal development of sea ice and its interaction with the ocean. For this you provide two, relatively old references, which are also not hitting the main point you want to make in your paper: That with spaceborne SAR one would be (perhaps) able to retrieve the sea ice thickness (SIT) distribution at finer spatial scale. I suggest, you try to find references which underline the present-day demand for fine spatial resolution SIT data. Possibly you find these in papers related to regional sea ice prediction for shipping etc.

Done. The introduction has been completely revised. For this part, we have emphasized the importance of retrieving the sea ice thickness distribution at finer spatial scale. And we have added papers related to regional sea ice prediction for marine transportation and offshore operations.

P5446, L22 to P5447, L6: This is an interesting mixture of different types of sensors from various platforms capable to obtain sea ice thickness estimates. I don't know what drove you to this selection but it is unstructured and not well organized. Again I suggest that you

structure the background information given here such that it leads to what you want to sell in this paper. For sure there is not the need to list and explain all SIT estimation sources but the list should make sense. A few comments to these: - Sonars measure draft from which sea ice thickness needs to be estimated via assumptions about buoyancy, densities and snow load. These exist in the Arctic and Antarctic in moored form and provide excellent information about the temporal development of SIT at one location. In the Arctic they have been also been employed from aboard submarines; the data archive from submarine sonar is actually our one and only data source about SIT in the central Arctic before satellite radar altimeters have been used to retrieve SIT. The one reference used here is not sufficient. - Electromagnetic induction sounders measure the total sea ice + snow thickness. There are sledge-based and fixed-wing aircraft versions of this technique which has been applied by various research groups - predominantly from AWI and in Canada. The two references given here aren't those I would use. In line 26 you switch without further notice to satellite data - leaving out in-situ measurements and air-borne SIT estimations such as provided by the Operation Ice Bridge campaigns. - When writing something about SMOS you need to mention that the SIT retrieval using this sensor is only possible for close to 100% sea ice cover and cold freezing conditions and level sea ice and is limited to SIT below about 30 cm to 50 cm over saline ice and below about 100 cm to 150 cm for brackish and/or MYI. - Then in Line 5 on page 5447 you cite a Kwok et al. paper - being still in the context of the SMOS explanations. This is not the correct reference. - Main sources for SIT retrieval from satellites are: ICESat-1 (this is where Kwok et al. papers fit), Envisat radar altimeter, ERS1/2 radar altimeter, CryoSat-2 and SARAL/AltiKa. Yes, they have problems to allow to retrieve fine spatiotemporal scale SIT ... but these are of different nature than of the SMOS sensor mentioned above. Enough of that. I guess the authors understand that this paragraph of the introduction is far from being complete and does not provide the motivation to the paper it should provide. L25: What is "sufficient accuracy"?

Done. The introduction has been completely revised. All suggestions by the reviewer have been considered. By introducing the limitations of different types of sensors, the motivation of the paper is provided.

P5447, L7: What is "much higher spatial resolution"?

Done. We specified this, range: 1-100 m.

P5447, L8: What is "all day"?

Done. It has been changed to "day-and-night".

P5447, L9: I guess this "almost all weather conditions" depends on the frequency used, correct? Again: "high spatial resolution" Please specify. Doesn't this come at the expense of the spatial coverage? Or do SAR images cover also swaths of about 1500 km width like satellite passive microwave sensors? You write further down about the limited swath width of quad- and dual-polarized SAR data but it would be nice to have a general info here as well. How about the temporal coverage? Does space-borne SAR allow daily monitoring of sea ice conditions at a certain location? It is important to mention these (current) limitations of SAR in advance. It would also be good to tell the readership what a SAR actually measures.

The information about spatial resolution, swath, temporal coverage and the current

limitations of SAR has been provided.

P5447, L10-18: Yes, a lot of work has been done here. Wouldn't it make sense to be more specific here and list which of the cited studies used L-, C- and/or X-Band SAR data? Which of these are based on satellite data and which on air-borne instruments? Which of these were developed and/or tested on Arctic sea ice? I suggest to spend an "e.g." in both lists of citations, i.e. in L11 and in L13 because there are many more studies. The sensitivity between co-polarization ratio and sea ice thickness for thin ice has been demonstrated e.g. by Onstott 1992 (in Book by Carsey, Microwave sea ice remote sensing). It is the later studies (cited here) which claimed that this is not only valid for thin ice but also for thicker sea ice.

Agreed. We considered these comments and added the required information.

P5447, L13: Do you mind to briefly explain what the co-polarization ratio is? L14: Do you mind to briefly explain what the "alpha angle" is? L19: Would you mind to briefly explain what the "cross-polarized ratio" is?

The co-polarization ratio and cross-polarized ratio are explained, but the alpha angle is not used in the modified text.

P5447, L22-23: Well, this isn't a conclusion really. In order to do so you would need to specify more what all the studies cited did. The benefit of using polarimetric SAR for sea ice classification and SIT retrieval may depend on the frequency and some parameters like the phase difference might be as important as the co- or cross-polarization ratio. I find also this part of the introduction not sufficient. The authors could have worked through the existing literature more carefully to embed their work better into what has been done.

We now specified radar frequencies, ice thickness ranges, and test areas. The major points to relate our work to what has been done before is clear now.

P5447, L24: Would you mind to give the polarizations which are usually used in "quad" and "dual" polarization mode data?

This is now already explained earlier in the introduction.

P5447, L29: I suggest to add an "(see below)" behind "SAR modes" to make clear that it will be explained further down what the CP mode actually is.

Done.

P5448, L10: "... calculated from CP mode SAR data."

Done.

P5448, L23: "first practical radar"? What is this? Is the Chandrayaan an Indian satellite?

Yes. We avoid this now and only mention RISAT, ALOS-2 and RCM.

P5448, L26/27: In order to avoid confusion, you could add a sentence that henceforth you will use "CP SAR" when you are referring to "CPLR mode SAR data".

Done.

P5449, Equation (1): You set $HV = VH$, correct?

Yes. Has been revised.

P5449, L15: Would you mind to explain that the subscript "R" is for right circular polarization?

The description of "R" is added.

P5450, L3: Perhaps "From Eq (3) it then follows that" ... ?

Yes. Done.

P5451, L3/4: One could add the typical RMS height and correlation lengths for this ice type here.

Done.

P5451, L10: One could add examples of the wavelength and SAR spatial resolution used in this paper.

We did.

P5452, Equation (9): What is "Erfc"?

The description of "Erfc" is added.

P5453, L17-L19: These results of the CP-ratio are then in line with the co-polarization ratio of "real" HH and VV-polarized radar backscatter values, aren't they? One could state this in the text.

Yes. We state this in the text.

P5454, L1: Is there any deeper motivation why the chosen incidence angles in Fig. 1 only vary between 30 and 50? Later, on P5456, L22 you speak of incidence angles between 20 and 60.

We now show results from 20° to 60°.

P5454, L3, How "realistic" is $\sigma < 0.15$? Is this a typical value for level first-year ice?

Sigma is the standard deviation of $\tan(\text{surface slope angle})$, i.e. $\sigma = 0.15$ is about 8.5 deg. No data exist about slopes of the facets on the ice. The extended Bragg model is conceptionally used here to provide a theoretical framework – one limitation is that actual measurements of sigma are lacking.

P5454, L5/6: Instead of "in most cases" one could write the conditions under which volume scattering can usually be neglected for first-year ice.

We mention the high salinity of arctic young and first-year ice.

P5454, L11: In the section ending here snow was not mentioned - as well as frost flowers on sea ice which might be incorporated in a snow cover. It would be good if there would be 1-2 sentences at the beginning of this section that it is assumed that the snow is transparent at the frequencies used and that eventual elevated salinities in the basal snow layer due to incorporated frost flowers will not have an influence.

We now explicitly mention these assumptions.

P5454, L24: Here sigma is the "standard deviation of the surface slope variation" while on P5453, L15 it was the "standard deviation of the surface slope"; on P5457 L4 one reads "standard deviation of the slope parameter". Which one is correct? I suggest to use the same description for sigma throughout the paper. Add ", respectively" after "H".

We corrected this ("standard deviation of surface slope") throughout the paper.

P5455, L3-6: You consider frost-flowers as potentially changing the small-scale surface roughness but at the same time you don't consider deformation processes. I wonder how this belongs together because frost-flowers grow on thin ice while deformation causing surface roughness components on the order of meters (vertically or horizontally?) are rather a process for thicker ice. Perhaps you could either give a lower SIT above which you carry out your investigations or you could be more specific here and describe how and if frost-flowers and the two deformation processes rafting and ridging are incorporated - if they are.

We now exclude frost flower growth and related surface roughness changes. The reason is that frost flowers require a completely different treatment of the radar backscattering. We explicitly mention this in the text.

P5455, L14: F_C is driven by the upward oceanic heat flux and the temperature at the ice underside. I assume you set it to the freezing point of sea water at which salinity?

The freezing point of the sea water we set as a constant -1.8°C . We explicitly mention this now.

P5456, L4-15: When I read this paragraph I get to know that the sea ice is grown under un-realistically constant conditions (23 days of constant temperature and wind). Does the sea ice grown like this really represent the physical property range that one would encounter in reality? Later in the paragraph you write that rms heights and correlation lengths were set to specific values? I initially hoped that employing the sea ice growth model was mainly motivated by trying to simulate the different (real) surface roughness conditions as a function of varying temperature and wind forcings. Maybe I overread a sentence in which you stated that the sea ice growth model is only used to get one realization of the ice internal parameters?

We note here that the paper demonstrates a first step for retrieving ice thickness using CP. This means that we start with ideal and simple conditions, considering the fact that we do not have field data of small- and large-scale ice properties available that would allow a very detailed analysis comprising various different scenarios. A question to the reviewer: is there any reference to a study that presents equations of the surface roughness as a function of wind and temperature?? We are not aware of such a study.

P5456, L26-P5457 L2: This statement surely holds but I am wondering whether this couldn't also be related to the discontinuity in the brine volume fraction in Figure 4 c) between day 4 and 5 (which is when H reaches 0.4 m) and the fact that the Cox and Weeks parameterization of the sea ice salinity has a discontinuity at $H = 0.4$ m.

Yes, we made this clear in the text

L5457, L5/6: "contribution of the ice-surface slope" ... perhaps you could also here stick to the same terminology that is used for sigma because the above phrase reads like it could be one small or large but constant surface slope but what you mean is the variability of the surface slope, am I correct?

Yes, the reviewer is correct. We have corrected this throughout this paper.

L5457, L5-8: I have difficulties to "read" the statement made here from Figure 6 for the entire SIT range shown. For SIT values up to the discontinuity at about 0.4 m indeed the CP-ratio decreases more with increasing SIT at low sigma than at high sigma. But at larger SIT values one can hardly see any difference in the slope of the graphs shown in Figure 6. How would Figure 6 look like for incidence angles 40, 50 and 60?

We also shown the case of 40° incidence angle, and we rephrased the text. The sensitivity of CP-Ratio to ice thickness is less at larger values of sigma. Given the same sigma values, the sensitivity of CP-Ratio is higher at larger than at smaller incidence angles. We mentioned those facts in the text.

L5457, L13: This reads fine but one could have added that the sensitivity is substantially larger for thinner sea ice (< 0.4m) than for thicker ice. Furthermore it becomes increasingly weaker the thicker the ice gets; the slopes in Figure 6 and 7 do not change even though the x-axis is in log scale. The CP-ratio changes between 0.5 m and 0.7 m SIT approximately twice as much as between 1.0 m and 1.2 m.

We mention this explicitly.

L5457, L25/26: I suggest to write "such soundings" when referring to earlier papers than the Prinsenberget al. one because you are referring to the accuracy of this measurement setting in more general here.

Done.

P5458, L4: You could add that the ground-penetrating radar allows to identify the ice-snow interface - and perhaps also the air-snow interface although the return is possibly weaker and the laser altimetry works better to define this surface - and therefore allows to retrieve the snow depth on sea ice.

Done.

P5458, L10/11: Where were the SAR images obtained from? In which processing step were they obtained (georeferenced, orthorectified, noise reduces, calibrated ...?)

They were ordered via MDA. Processing steps are now described.

P5458, L11: Perhaps write "field survey" instead of "measurement"? Does your readership know what a Pauli RGB image is?

Regarding "field survey": done. About "Rauli RGB", we think not all readers will know what in detail a Rauli RGB image is. In this case we expect that the readers check themselves since this term is explained in many textbooks about polarimetry and decomposition.

P5458, L22: "footprint of EM" -> "footprint of the EMS"

Done.

P5459, L1: How were open water regions defined?

The definition of water regions focused on dark areas, and the interpretation was based on the backscattering signature and texture features. We note that areas with a thickness < 0.1 m (measured by the EMS) are anyway not considered in the analysis, which alleviates any potential errors in the detection of open water areas. This is mentioned in the text.

P5459, L5/6: Would you think that it might make sense to share the criteria used to exclude deformed ice from the analysis by using the laser data? I can imagine that you computed something like standard deviation of the surface slope and correlation length?

The criteria are described in step 4 of the processing chain, section 4.2.

P5459, L7-10: I have few questions here: - How accurate is the GPR-based snow depth retrieval over level sea ice? - Does the history of the snow pack development suggest that it is a "smooth" one without substantial changes in density and/or grain size due to melt-refreeze events and/or depth hoar growth? - Would you mind to share how many data points you needed to exclude due to too high snow load? This last question also applies to the surface types left out from step 3 of your processing chain. I see that you tell at the end of this section that the total length of the useful profiles is 10 km (702) samples. OK, but what was the original number? Where 1, 5, 10 or 50% of the original data discarded? This is an important information for the planning of future surveys.

The information of GPR-based snow depth retrieval (section 4.1) and snow properties (section 4.2) are now provided. The reviewer shouldn't forget that we rely on the information given in the field survey report. We provide information about the percentage of data points that could not be used since they did not meet the criteria given in the processing chain section 4.2.

P5459, L12/13: How did you decide whether there is just one ice type in these areas?

Using the segmentation procedure, it is rather to segment the radar signature into homogeneous area (in which the radar signatures of all pixel are statistically equivalent). We assume that each segment represents homogeneous ice conditions. We mention this in the text.

P5459, L14: I don't fully understand the reason for this 13 x 13 pixel window. All helicopter-based data are only obtained along the track, right? I recall: Laser every 3-4 m with a footprint of several centimeters; EM every 3-4 m with a footprint of 20 m; GPR every 1-1.5m with unknown footprint. The SAR images have 8 m pixel resolution. Therefore we have 4 different sample spacings and I am wondering to which the 13 x 13 pixel window applies. As you write that this corresponds to 50 m on the ground I assume that you are taking the sampling distance of EM and laser as the basis. But this means that you average over i) 6-7 SAR pixels, ii) 13 completely independent laser samples, iii) 13 highly correlated EMS samples.

We explained this in more detail, see step 5 Section 4.2. The window is used for segmentation of the SAR images.

P5459, L20-21: *It would be good (see above) if you can underline that the chosen sea ice patches have a $\sigma < 0.15$.*

How? We do not have corresponding field data. We think that the helicopter measurements are too coarse (flight attitude and altitude variations) and the laser accuracy not high enough to get reliable values on σ (slope).

P5460, L7-9: *This one way of seeing it. One can also say: Figure 10 illustrates that with a CP-ratio of 0.4 it is very likely to obtain a sea ice thickness between 5 cm and 20 cm. With a CP-ratio of 0.2, however, SIT values can range between 0.3 m and 3.5 m. ... How much work would it be to derive a plot where you show a histograms of SIT values for CP-ratio bins? I mean, the measured parameter is the CP-ratio and it would be very informative to see down to which CP-ratio value one has a reasonably narrow SIT range and/or a reasonable concentration of the single SIT values around an average SIT value (would also apply to Figure 11 perhaps). There is an inconsistency in SIT ranges shown in Figures 10-11 (start at 0.0 m) and those given in Figures 5-7 (minimum SIT = 0.2 m). This leaves the question open whether the observed further increase of CP-ratio towards smaller SIT values holds also from the theoretical considerations shown in Figures 5-7. Yes, I am aware of the fact that you discarded observed SIT < 0.1 m because of the limitations of the EMS system. This leaves the range between 0.1 m and 0.2 m open for discussion - in particular in the light of the slight discontinuity in the CP-ratio SIT relationship at SIT values < 25 cm towards incidence angles of 50 and 60.*

We think that Figs. 7-9 offer the opportunity to estimate the range of uncertainty in thickness retrieval because of unknown small-scale roughness and surface slope, and – if a snow layer is present – because of the unknown incidence angle on the ice surface. We do not present a new figure because we have already many of them...

Please note that the x-axes scales in Figs. 5-7 are logarithmic, and in Fig. 10 the x-axis is in linear scale. We do not understand the point addressing the “slight discontinuity” at SIT values < 25 cm.

P5460, L8-11: *You mention the presence of multiyear ice (MYI) here as one of the possible factors for the reduced sensitivity to SIT shown in Figure 10. Do you have evidence that MYI was indeed present in the region of interest? I mean, MYI does sometimes drift along the Western shores of the Labrador Sea southward. But it would be good if you could underline - e.g. by means of Canadian Ice Charts whether this really is the case. If not then your process to discard deformed sea ice described earlier did not work properly. In general, I am quite surprised by the relatively large amount of sea ice thicker than about 1.2 to 1.6 meters which I would assume is the maximum possible thermodynamically grown first-year ice in that region - except perhaps in some of the enclosed bays with fast ice coverage. But also there I doubt that SIT is exceeding 2 meters from pure thermodynamic growth. In addition, in your explanation why MYI causes a reduction in the sensitivity of the CP-ratio to SIT you only comment on the lower and vertically constant salinity but you do not comment on the increased porosity which causes a substantial amount of volume scattering which eventually exceeds the fraction of surface scattering.*

Because of the new processing chain and the careful separation of level and deformed ice, we did not obtain ice thickness values > 2.2 m for the profile data that passed the threshold

in the processing chain. Hence we can exclude the presence of MY ice along our profiles.

P5460, L17: I suggest to write 0.05 m and 0.78 for RMS error and correlation, respectively. I wouldn't give the RMS error with more decimals than the accuracy of the retrieval could theoretically be on average and I don't think that you are able to retrieve SIT with a better accuracy than 1 cm.

Agreed. We have corrected it.

P5460, L18: I don't see a reason why the "and can hence be ..." part of the sentence needs to be in "()".

Done.

P5460, L20: I suggest to refer to Table 3 here. Figure 11: What could be the reason that the regression lines have a larger distance for the two higher incidence angle cases (42 and 49) with an incidence angle difference of just 7 than for between the lines for 29 and 42 incidence angles with an almost twice as larger incidence angle difference?

Table 3 has been referred and the figure has been updated.

P5461, L6-14: - I assume that path-3 which is overlapping with both image #1 and image #2 is the one from which the EMS data are used here. This needs to be written and also referenced to Table 3 and Figure 8. It needs also to be mentioned that you limited the SIT retrieval using the CP-ratio to those 50 m transect pieces in the SAR image which fulfil the criteria mentioned on page 5459. - How many data points do we see in Figure 12? - As the number of data points is relatively small: It would not hurt to give an uncertainty estimate for each of these data points, i.e. an error bar. I mean, the agreement is perfect but would get even higher credibility with error bars. - I would write 8 cm and 20% instead of 8.05 cm and 19.95% for the absolute and relative RMS error, respectively. Does the mentioning of the relative RMS error imply that the absolute RMS error is 0.2 m at a SIT of 1.0 m and 0.02 m at a SIT=0.1m? If so, then I recommend to mention this explicitly.

Now, we consider all the comments, explain these explicitly, and the figure has been updated.

P5461, L23: If I have understood it correctly, then you evaluated your method with one SAR image (image #2) not with several ones.

Two images (#2 and #3) were used to evaluate our method. We mention this in the text now.

P5461, L25 - P5462, L1: see above with respect to number of decimal digits.

Done.

P5462, L1/2: Yes, I agree, the method is useful but it is essential to mention i) during freezing conditions, ii) for snow depth < 0.2 m, iii) at C-Band frequencies.

Agreed. We have mentioned them.

P5462, L3-7: This paragraph might need to be re-written depending on your answers towards comments towards L8-11 on P5460 and L5-6 on P5459.

This sentence has been removed.

P5462, L8 - P5463, L3 and Figure 13: In the light of the main results of the paper, of the need to extend the introduction / motivation and being a bit more detailed here and there when it comes to the interpretation of the results I suggest to skip this part and figure. We have skipped this part and figure

P5463, L3-9: You could be more specific here and perhaps mention Sentinel-1A/B? You could also comment on the applicability of your method to data from SAR sensors operating at other frequencies such as L-Band (PAL SAR) or X-Band (COSMO- Skymed, TerraSAR-X).

We mention satellites with CP-capabilities in the introduction. Any comments regarding other frequency bands and their potential with CP are speculative at this stage and may be the topic of a future study.

P5463, L9: I am sure more can be said in this section. I am naively giving a few comments / asking a few questions in the following to show you how - at least my brain - would work. - You test your algorithm for a SAR image subset from which you know from auxiliary data where you have level first-year ice and where your snow depth is < 20 cm. What actions would be required to simply take the CP-ratio of an entire SAR image to derive the SIT? This is a question of practical matters. Where would you get the required information from? How would you deal with the incidence angle range encountered across the 350 km wide images? How would a practical implementation look like? Would one need to classify the image first? Would one carry out a correction for the incidence angle variation before applying your method? Would one need to find an empirical relationship for every SAR image or is there the potential to prepare a look- up table for these? - What are the limitations of your approach with regard to processes changing the snow properties towards being less transparent? What are the limitations of your approach with regard to ocean-sea ice-snow interaction processes where the basal snow layer properties / ice-snow interface properties are changed e.g. by re- freezing slush, wicked up brine, hoar frost development etc.? - What I also miss is more discussion about whether the environmental conditions and or the choice of the model parameters could have had an impact on the results. Examples for this could be the very constant ice growth simulated, and the varying differences between EMS measurements and SAR image acquisitions.

We agree that practical issues need to be solved and discussed in more detail. The reviewer can be sure that our brains work in similar ways. However, our paper is already lengthy, and we are of the opinion that the practical issues have to be addressed in a separate study. Regarding the effect of environmental conditions, we touched a few details about the influence of snow but note that this issue needs to be addressed also in more detail in future work.

The choice of the models (which may be even more critical than the choice of model parameters) again is worth a separate study. In this case, we acted as “end-users” who need to decide which model is most appropriate in view of the parameters that can be determined by measurements.

P5464: L14 & L19 % L28: "T." -> "Trans.", "Sens." missing -> this occurs on the other pages as well. L18: "olarimetric" -> "polarimetric"

Done.

Figure 1 & 2 & 4: I find the font size of the axes annotations and the legend quite small - in particular in comparison to the size of the figures.

Done.

Figure 6: I suggest to change the first sentence of the caption to: "Sensitivity of the CP-ratio to the standard deviation of the surface slope sigma (x-axis ..."

Done.

Figure 7: - Why is this for 40, 50, and 60 incidence angles? What about 20 and 30 which are used in Figure 6? I suggest to change the first sentence of the caption according to the style in Figure 6: "Sensitivity of the CP-ratio to small scale surface roughness (x-axis ..."
- I find the blue and black lines very difficult to discriminate. Perhaps you could use cyan instead of blue?

We now show results from 20° to 60°, and all the comments are considered.

Figure 8: - You could have chosen a Canadian Ice Service Ice chart as a background or something else other than Google maps. Or a simple sea ice concentration map. Perhaps a more simple map with land, coast and open water without the unnecessary details given in the Google maps about topography on land and under water would do it as well. I find it confusing this way. - If you keep the map as it is I recommend to choose grey frames for the SAR images and then draw the path-8 in white. It will be visible better against the grey texture of the SAR image in the background. - I would also give the day and time of the SAR image acquisition in the figure caption. Or you refer the Table 3.

The figure has been updated, and all the comments are considered.

Figure 9: You could be more specific about the "averaged" in the caption. If I have understood it correctly then every single SIT value is representative of a 50 m long transect piece.

Yes. The figure has been updated.

Figure 10: - You could also use a logarithmic X-axis scale like in Figures 5 to 7 (this applies also to Figure 11). - What is the number of data points shown? 702? - I would only shade the confidence interval and don't show the bordering dashed lines. Caption: I suggest to write: "CP-ratio derived from the SAR images as a function of the sea ice thickness derived from the helicopter-borne field survey. The red line denotes the logarithmic best-fit regression derived from the data. The shaded area corresponds to the 90% confidence interval around the regression."

This figure has been removed.

Figure 11: Here the discrimination between blue and black is easier due to the shading of the confidence intervals (compare my comment to Figure 7) - Why did you use 50% for the confidence interval here and not 90% like in Figure 10? - There is another very narrow, darker shaded area around the regression lines. What is this?

The figure has been updated.

Figure 12: Fonts are clearly too small.
Corrected.

Typos: P5447: L8: "Synthetic aperture radar" -> "Synthetic Aperture Radar" P5448: L4: "making it is well" -> "making it well" P5451: L12: "whereat" -> "where at" P5457: L13: "underformed" -> "undeformed" P5458: L17: "time difference" -> "time differences"
Done.

Part II

To the editor and reviewer 2:

We have revised the paper to address the main issues raised by the reviewers, as well as to include minor modifications of the authors. In the following list, we first address the major issues that are of importance in general, then we refer to the issues raised by reviewer 1. The major revisions of this paper including 4 parts:

- (1) We reorganized Section 1 "Introduction". We emphasized the significance of retrieving the sea ice thickness distribution from CP SAR both in the ice services and sea ice forecasting. And an overview of the differences between dual-, quad- and compact-polarimetric modes was provided.
- (2) In section 3 "Simulation", we carefully discuss the effect of snow layer, and we used real scenario roughness parameters to evaluate the rough surface scattering contribution now.
- (3) For data process in Section 4.2, the processing chains were described detailed. The procedure of ice drift correction was provided. The method of segmentation level and deformed ice was modified, the new processing chain can exclude deformed ice, and the ice thickness values > 2.2 m has been passed.
- (4) The limitations (including snow layer and environment conditions) and outlook of our method was descried and discussed.

Detailed response to the reviewers' comments is below. Reviewers' comments are in italic immediately followed by our response.

General Comments

This paper provides, to my knowledge, the first attempt at retrieving sea ice thickness from (simulated) compact polarimetric (CP) synthetic aperture radar (SAR) data. The authors introduce a CP parameter, the CP-Ratio, which shows considerable promise for the retrieval of level first-year sea ice (FYI) thickness from C-band CP SAR data. The authors

provide the theoretical framework to demonstrate that the CP-Ratio is sensitive to the dielectric constant and surface roughness of sea ice and to the incidence angle of observation. Through numerical model simulations, it is shown that over level FYI the CP-Ratio is sensitive to the dielectric constant, which is primarily a function of salinity, which in turn is strongly related to the ice thickness, assuming purely thermodynamic growth. Empirical relationships between the CP-Ratio (calculated from quad-pol RADARSAT-2 images) and airborne measurements of FYI thickness (derived from electromagnetic induction sounding) are shown to have a strong correlations using an exponential fit. Using a single RADARSAT-2 image as validation the authors demonstrate that their method can produce accurate sea ice thickness retrievals.

This paper is well suited for the scope of TC, and presents a novel method for inverting FYI thickness from SAR data that may have significant impacts on the sea ice community, particularly for operational sea ice monitoring. I believe it represents significant progress in this field. However, the paper requires some improvements:

1) The authors need to better define the target audience of this work in the introduction and need to outline relevant user requirements (e.g. spatial resolution, temporal revisit time, swath width etc.) for SAR derived ice thickness products. Ice services, who currently utilize SAR data in an operational context to map ice conditions in near-real time are the obvious stakeholder that would directly benefit from SAR derived ice thickness estimates from CP SAR data. This should be outlined at the very beginning of the introduction. Other possible user groups (e.g. sea ice modelers/forecasters) also need to be identified. The authors repeatedly mention that higher spatial observations of ice thickness are needed, but not all applications (e.g. sea ice climate modeling) require data at the high spatial resolution provided by SAR observations. Revisions are also needed in the conclusions to directly relate the significance of the results to the various possible users of SAR derived ice thickness products.

2) Compact polarimetry is still a relatively novel method of SAR data acquisition (at least for Earth Observation SAR missions) that many readers are likely to be unfamiliar with. It would be beneficial if the authors provided a brief overview of the differences between dual-, quad- and compact-polarimetric beam modes earlier in the introduction to familiarize the readers with the benefits of CP beam modes. In particular, the authors should explain how CP is able to provide increased swath widths and spatial resolution relative to 'standard' quad-pol data.

3) Further discussion on the impact of sea ice drift on the results is required. The authors do acknowledge that ice drift is likely to have an impact on the correlations observed between the CP-Ratio and airborne ice thickness measurements; however, they do not attempt to apply a correction to account for the ice drift between the acquisition times of the SAR data and the airborne electromagnetic induction sounding (EMS) data. Presumably this is due to an absence of ice drift data. However, in the Labrador Sea ice drift can be very fast (up to tens of kilometers per day), as evidenced by buoy data illustrated in Fig 30 of the DFO field campaign report (Prinsenberget al., 2012). Aside from EMS surveys P-4 and P-5, at least 4 hours and up to 26 hours passed between the acquisition times of the EMS and SAR data sets. In these cases, it is unreasonable to assume that the SAR data and EMS measurement lines observed the same ice floes. I am impressed by the results presented in Section 4, but am skeptical of how such strong results were achieved given that significant ice drift would have occurred between the SAR and EMS

data acquisitions. The authors must provide some justification for why they did not attempt to correct for ice drift, or if they did do so, the methods used need to be described in detail. In this version, we reorganized Section 1 “Introduction”. Besides we emphasized the significance of retrieving the sea ice thickness distribution from CP SAR both in the ice services and sea ice forecasting, we provided an overview of the differences between dual-, quad- and compact-polarimetric mode, and explained why the CP mode can increase swath widths. Because of the extensive changes we made in the introduction, it is difficult to relate single parts of the modified text to the old text. The new introduction should be read in its entirety. Lastly, we presented the procedure of ice drift correction, and the detail description is given in section 4.2.

Specific Comments

P5445, Title: The title could be modified slightly to “. . . from simulated C-band compact polarimetric SAR images” to indicate that the data used are not true compact polarimetric data, but rather are simulated from quad-pol data.

Done.

P5446, L6-7: What are the “optimal conditions for thickness retrieval”? They should be stated in the abstract as concisely as possible.

The "optimal conditions" means optimal sea ice conditions and radar parameters. Thanks, has been changed.

P5446, L14: I think it would be more appropriate to state the range of ice thicknesses across which the RMSE and correlation coefficients were calculated (0.1 to 1.5 m) rather than the mean; or better yet state both the mean thickness and thickness range.

We considered these comments and explicitly mentioned these in the text.

P5446, L16-21: The first paragraph of the introduction is far too brief. The authors need to elaborate on why knowledge of the ice thickness distribution is of interest to a wider range of user groups and why it is important to other science questions. E.g. the authors do not mention the importance of sea ice thickness for model forecasts of sea ice conditions (both seasonal and long-term climate forecasts) or to support polar operations (marine navigation, resource exploration and extraction etc).

Done. The introduction has been completely revised. For this part, we have emphasized the importance of retrieving the sea ice thickness for model forecasts and polar operations

P5446, L22-24: The authors fail to include several methods that have been used to measure sea ice thickness including: in situ measurement techniques (drill holes, ground based EM surveys); and, more importantly, airborne and satellite altimetry (e.g. ICESat, Ice- Bridge and CryoSat-2), which has been used to provide pan-Arctic estimates of ice thickness.

The introduction has been completely revised. This part has been reorganized, all comments has been included. By introducing the limitations of different types (including drill holes, EMS, and altimetry) of sensors, the motivation of the paper is provided.

P5447, L5: The reference to Kwok et al (2009) is inappropriate. Kwok et al discuss Arctic sea ice thinning and volume loss estimated from ICESat – it does not mention radiometer

derived ice thicknesses at any point. At what resolution are radiometer derived sea ice thickness products provided? 25 km? For what users would this resolution be considered coarse? For many applications (e.g. climate modeling) ice thicknesses at these coarse resolutions would be sufficient.

We have revised these and the specific information of radiometer has been added.

P5447, L6-10: Related to the previous comment, what do you mean by higher resolution? 1 km or 100 m or 10 m? If possible provide the spatial resolution expected for compact-pol SAR beam modes (100 m?).

The information is now provided

P5447, L11-12: It would be useful to also separate the list of references provided here by the radar frequency bands considered in each study. Most of the references cited analyzed L-band SAR data, which should be noted.

The information is now included.

P5447, L24: Define what quad- and dual-polarization modes are.

This is now already explained earlier in the introduction.

P5447, L24-26: Again, you need to define what the user requirements are that you are trying to meet. What is the areal coverage required by your targeted audience/user base? Is a 500 km swath wide enough?

We separate science users and operational mapping. There is now rule-of-thumb for the optimal swath width. It depends on the application. We think it is beyond the scope of this paper to discuss this in detail.

P5447, L26-27: RADARSAT-2 has “wide fine quad-pol” and “wide standard quad-pol” modes that provide 50 km swath widths. See Page 2-8 of the R-2 Product Description document: http://gs.mdacorporation.com/includes/documents/RN-SP-52-1238%20RS-2%20Product%20Description%201-8_15APR2011.pdf

Thanks, we considered this.

P5447, L28: It should be noted that some SARs (RADARSAT-2, Sentinel-1A, and PALSAR-2), can acquire dual-polarized data at ScanSAR beam modes.

We mention this explicitly for RADARSAT-2.

P5447, L28-P5448, L2: Some readers may be unfamiliar with compact polarimetry. It would be beneficial if you could include a sentence or brief paragraph explaining the difference between CP and traditional linear polarimetric systems (e.g. CP transmits a circularly polarized wave, and receives H+V linear backscatter, allowing acquisitions over a wider swath width at higher resolution, relative to traditional quad-pol beam modes, through reduced power consumption and data storage requirements).

We have modified these as suggested.

P5448, L2: You should note that CP modes will provide a reduced quantity of polarimetric information relative to quad-pol modes.

Yes, we clarified this.

P5448, L3: Salberg et al (2014) is not an appropriate reference. Salberg et al do not outline forthcoming SAR missions that support compact-pol modes. Find another source if possible, or simply to state the names of current/future sensors that will support CP (e.g. RCM, PALSAR-2).

We stated the names as suggested.

P5448, L5: Operational sea ice monitoring, which is the stakeholder that could best take advantage of the results of this work, needs to be mentioned much earlier in the introduction. It should be outlined from the first paragraph that operational sea ice monitoring would benefit greatly from sea ice thickness derived from SAR data.

We did this.

P5449, L18: I don't think it is accurate to state "two orthogonal circular polarizations", I think this should be "two opposite handed circular polarizations".

It is possible to use the term "orthogonal circular polarizations. But we avoided this term in the new version of the paper.

P5449, L19-20: Following the convention in Nord et al (2009) CTRLR is an acronym for "Circular Transmit, Linear (horizontal and vertical) Receive". You should use this explicit definition, as the current text leads the reader to wonder why "L" is included in the acronym.

The meaning of CTRLR is explained in the introduction and in the abstract

P5449, L23: What do you mean by the "first practical radar"?

The "first practical radar" is the Chandrayaan satellite. We avoid this now and mention Risat, ALOS-2 and RCM, see above.

P5451, L4: What are typical values for the RMS height and correlation length of smooth FYI? Include appropriate references.

We provided examples.

P5453, L17: Provide a reference for the value of the dielectric constant of FYI that you have used here.

Done.

P5454, L16-19: Can you explain why you didn't use the surface scattering term from the Nghiem et al model? Why did you use the PTSM model of Iodice et al instead?

Nghiem et al consider SPM as well as physical optics (PO) and geometrical optics (GO). The disadvantage of SPM is explained in our text. The applicability of PO for sea ice was critically discussed in the late 70s, and most simulations are now carried out with the IEM and its extensions (not use by Nghiem). Since the extended IEM is too complex in particular for retrievals of geophysical parameters, we decided to use a more straightforward approach by applying PTSM.

P5454, L20 to P5455L2: The organization of this paragraph could be improved. I recommend introducing all of the permittivity parameters first (air, water, ice and brine), then introduce the surface roughness parameters. You also need to add a definition for the permeability μ_0 , which is shown in Fig. 3 but not described in the text.

Thanks. All the comments have been considered.

P5454, L22: Is only the ice surface (top) roughness defined? If the ice bottom roughness is also prescribed in the model, specify that here, and add relevant labels to Fig 3.

We do not consider the scattering contribution from the ice-water interface (because of the high salinity of arctic young and first-year ice), which is now mentioned in the text.

P5455, L4-6: Do you mean you do not consider deformation processes that are dynamic in origin (i.e. rafting/ridging)? Some dynamic processes (e.g. rafting of nilas) can cause deformation on centimeter to decimeter scales.

We do not consider deformation processes. The simulations are for ideal cases (as in most other studies). We mention this in the discussion.

P5455, L12-17: define the symbols used in Eq. (13) in the same order in which those terms are found in the equation so that it is easier for the reader to follow along (i.e. define α first, then F_r , then I_0 etc.)

Done.

P5456, L1-2: What are the valid ranges for s , l and σ within the X-SPM model? It would be helpful to provide these to the reader. Furthermore, references should be provided to demonstrate that the range of values considered for these parameters are representative of FYI surfaces.

References for the X-SPM ranges are given, the selected parameters represent the validity range. FY-Ice roughness: see section 2.2, where typical values for level ice are given based on the Fung reference.

P5456, L6-7: Why were these fixed values of air temperature and wind speed selected? You need to provide justification for these values. Are data available for a weather station near the study region? Check Environment Canada's climate data archive (<http://climate.weather.gc.ca/>), I believe there is a station at Makkovik.

Data are based on information from the field campaign described in Section 4 – we now mention this here.

P5456, L13-15: Again justification is required for the values of s , l and σ . Provide references to demonstrate that the chosen values are typical for FYI. You also need to provide a definition for the wavenumber symbol k .

The small-scale roughness validity ranges of the Iodice-model are not given explicitly. We use the Bragg-backscattering validity range which should be acceptable for the Iodice model. The used small-scale roughness parameters are based on the data reported in Onstott, 1992; page 86, table 5-3. we explained what “k” means.

P5456, L24-26: The impact of ice thickness on CP-Ratio was not discussed in Sect. 2.

Thanks. This was an error, we removed the hint to section 2.

P5457, L10: when you state “more or less independent of the incidence angle” do you mean CP-Ratio is not sensitive to incidence angle? It seems clear to me that CP-Ratio is highly dependent on incidence angle.

The reviewer is right, we changed the text accordingly.

P5457, L13: The impact of incidence angle on the CP-Ratio should be acknowledged here. I would change this sentence to read: “. . . has a strong correlation with the thickness of smooth undeformed ice at any given incidence angle.”

The reviewer is right, we changed the text accordingly.

P5457, L18-19: Indicate the data source for these air temperature and wind speed measurements.

Temperature and wind data are now discussed in section 4.2, and the reference is included

P5457, L26: Remove the reference to Simila et al (2010). That paper references Haas et al (2006), which you have already cited. Also remove the Simila citation on P5458 L3. Instead add the following reference, which discusses the calibration and accuracy of the EMS system used by DFO: Prinsenberg, S., S. Hollady, and J. Lee (2012). Measuring ice thickness with EISflow, a fixed-mounted helicopter electromagnetic-laser system. Proc. 12th International Off- shore and Polar Engineering Conference, 1, 737-740.

Done.

P5458, L4-5: Change this sentence to read “By subtracting the GPR snow thickness measurements from the EMS snow plus ice thickness measurements, sea ice thickness can be estimated.”

Done.

P5458, L11: change “the measurement” to “the DFO airborne survey flight lines”

Done.

P5458, L11-12: Define what a Pauli RGB image is.

The definition of a “Pauli RGB” is given in Fig. 8.

P5458, L16-19: As outlined in my general comments, further discussion is required regarding the potential impact of ice drift on your results, as only 1 SAR image was acquired within an hour of a coincident EMS survey. In the DFO field report (Prinsenberg et al., 2012) Fig. 30 shows drift tracks for icebergs and ice floes acquired by ice beacons during the field campaign. This figure indicates that ice drift was on the order of tens of kilometres per day! To me, this indicates that in all cases you cannot reasonably assume that the SAR pixels located underneath the EMS flight lines observed the same ice floes as were observed during the EMS surveys. Was any ice drift correction applied to (automatically or manually) co-locate the SAR and EMS datasets? If so this must be described in detail in the manuscript. If not you must provide an explanation for how you have any confidence that the SAR and EMS were observing the same ice.

We provided the description about ice drift correction. The procedure is described in section 4.2.

L19 and L26: specify "spatial resolution".
Done.

P5459, L1-19: I think the 7 data processing steps should be described with more detail. I found several steps to be unclear (see following comments). L5-6: How were deformed ice and icebergs identified? Was this done manually/visually? Where any automated procedures applied? What criteria were used to determine if sea ice is deformed? L7-10: Provide more suitable references to support your 20 cm threshold for snow depth. . . Stiles and Ulaby (1980) discuss the impact of snow wetness, not snow depth, on microwave response. Nakamura et al (2009) evaluate X- and L-band SAR backscatter over sea ice, so their results cannot be directly applied to C-band. Both these references should be removed. L11-15: How do you determine that only one ice type is present within an area? Are you manually delineating individual ice floes?... When averaging the airborne data, are they always averaged in 50 m sections? Or does each section simply need to be at least 50 m long (e.g. can one profile segment be 50 m in length and another be 100 m?). The profile segments should have a constant length. L22: If you have 702 samples, each at least 50 m in length, that should total at least 35 km, not 10 km as indicated in the text. Please correct/explain this discrepancy. L24: The maximum ice thickness for a profile segment is reported as 3.3 m. It is not realistic for FYI in this region to grow thicker than 2 m through thermodynamic processes alone. To me, this indicates that at least some of the profile segments include deformed ice. Some discussion of why ice thicknesses greater than 2 m are observed should be provided, or perhaps the masking of deformed ice requires improvement?

We modified the processing change and hence the description of the different steps. We tried to consider all items listed by the reviewer.

P5460, L5, Fig. 10: Are all 702 data points plotted? It doesn't look to me like there are 702 data points shown in Fig. 10. . . additionally, is Eq. (14) derived using all 702 data points? or a subset of the ice thickness and SAR datasets? The SAR images and EMS paths included in these figures/regressions need to be made explicitly clear.

Now 320 data points are left, and we mentioned this in the text

P5460, L8-9: You state that ice thicknesses exceeding 2 m correspond to multi-year ice (MYI); however, Canadian Ice Service (CIS) charts do not indicate the presence of MYI along any of the flight lines. Can you identify MYI with certainty in the quad-pol SAR data? Are you sure these aren't simply areas of deformed ice? CIS charts are available from: <http://iceweb1.cis.ec.gc.ca/Archive/?lang=en>

Because of the new processing chain and the careful separation of level and deformed ice, we did not obtain ice thickness values > 2.2 m for the profile data that passed the threshold in the processing chain. Hence we can exclude the presence of MY ice along our profiles.

P5460, L9-11: While the dielectric constant of MYI is unlikely to change significantly with ice thickness, backscatter from MYI is dominated by volume scattering, not Bragg

scattering, and the surface roughness of MYI is much greater than that of FYI, so the assumptions used when modeling CP-Ratio versus ice thickness cannot be applied to regions of MYI. These considerations should be discussed, assuming MYI is proven to be present.

Now the MY ice has been excluded, see above, and hence it is not necessary to discuss the effect of MY ice.

P5460, L17: provide units for your RMS error (this applies throughout the manuscript). The RMSE and CC are also provided at far higher precision than is justifiable given the uncertainty of the EMS thickness measurements (at best cm precision).

We considered this

P5460, L18-19: While this equation can be applied without knowing incidence angle – is that a wise thing to do? I doubt that this empirical equation would provide useful results if applied to a different scene let alone a different study area or study year.

The equation has been removed.

P5460, L25, Eq. (15): Again are all data points (grouped by incidence angle) used to derive these empirical regressions? Or are only some flight segments/images used?

Now we explain this explicitly.

P5461, L1-2: this statement is too general. You need to specify that this will work for “smooth level first-year ice from C-band radar images, under winter dry snow conditions.”

Done

P5461, L13-14: For the validation work presented in this paragraph, your results are limited to thicknesses < 1.5 m. Why have you subset your validation dataset to < 1.5 m while the preceding paragraphs included all data points (up to 3.3 m)? L14: Can you also include the mean bias for the validation dataset.

Now we explain this explicitly.

P5461, L23: Sentence needs to be edited, you state RADARSAT-2 images (plural), were used for validation; however, only one validation image was presented.

Done. Two images (#2 and #3) were used to evaluate our method and we explain this explicitly.

P5462, L2: While the first paragraph of Sect. 5 does a reasonable job of summarizing this work, some important details should be acknowledged. First, it needs to be stressed that the results are derived from a single field campaign with a limited number of SAR images, spanning one study site and only two days. Further validation work is required before the regression equations presented can be applied in an operational context. Second, further work is needed to define thickness inversion equations at other incidence angles. Finally, the valid range for ice roughness (σ , l , and rms height) and snow conditions (< 20 cm, dry snow) in which these results can be considered applicable, should be explicitly restated here.

We agree that practical issues need to be solved and discussed in more detail. The reviewer

can be sure that our brains work in similar ways. However, our paper is already lengthy, and we are of the opinion that the practical issues have to be addressed in a separate study. Regarding the effect of environmental conditions, we touched a few details about the influence of snow but note that this issue needs to be addressed also in more detail in future work.

The choice of the models (which may be even more critical than the choice of model parameters) again is worth a separate study. In this case, we acted as “end-users” who need to decide which model is most appropriate in view of the parameters that can be determined by measurements.

P5462, L9-11: You should note that the relationship between large-scale surface roughness and ice thickness reported by Toyota et al (2009) and Peterson et al (2008) is for FYI. Neither study included MYI. L15: Define a symbol for the correlation coefficient between ΣH and ΣV - perhaps ρ_{CP} ? Then use this symbol in Eq. (17) and Fig. 13.

We have skipped this part and figure.

P5463, L5: specify that “C-band compact polarimetric SAR has great potential for sea ice thickness retrievals over level FYI cover by a thin, dry snowpack.”

Done.

P5463, L6: mention what current/planned C-band SAR missions support compact-pol data acquisitions. Also it would be great, if possible, to provide some comments on the possible use of compact pol data at other frequencies (specifically L-band or X-band).

We mention satellites with CP-capabilities in the introduction. Any comments regarding other frequency bands and their potential with CP are speculative at this stage and may be the topic of a future study.

P5463, L9: what about other applications/user groups aside from operational ice monitoring (e.g. seasonal and climate sea ice forecasting) – could they benefit from this work?

We address this point at the end of Section 5.

Table 3: Number and order the RADARSAT-2 scenes chronologically. Change the caption to read “Specifications of the quad-pol RADARSAT-2 data” and remove the Polarization column from the table. In the column headers fix the following typos: “Data/Time” to “Date/Time” “Resolutions” to “Resolution” “Incident” to “Incidence” The spatial resolution of RADARSAT-2 SLC data products varies with beam mode and is not constant in the range and azimuth directions – have you resampled the data to produce square pixels? If so you need to explain this in text. If not both the range and azimuth resolutions should be listed.

The table has been updated, and all the comments are considered.

Table 4: Replace “EM” with “EMS” throughout the table (caption and table headings) – be consistent with the use of abbreviations/acronyms provided in the text. In the table headings change: “SAR data coincident with EM” to “SAR Scene ID coincident with EMS” “Data/Time” to “Date/Time” As with Table 3, number your EMS flight segments

chronologically.

The table has been updated, and all the comments are considered.

Fig 1: Add a line on the plot for incidence angle = 20 degrees (wide swath beam modes for Earth Observing SAR sensors typically range from 20 to 50 degrees).

For consistent the incidence angles in all our figures, we now show results from 20° to 60°.

Fig 2: It would be helpful to mention in the text whether or not the results for other incidence angles follow similar trends as those shown for 30 degrees. Also why does the x-axis cover such a large range? The dielectric constant of FYI should cover a much smaller range of values near 3.

We gave the results only the value of dielectric constant near 3.

Fig. 4: The font size of the axis labels and tick marks is far too small to read. I would also recommend that you try combining these three plots into a single plot with multiple y-axes and three different colored lines instead of three separate graphs. Adding grid lines to the plots would also be helpful (this goes for all graphs in the manuscript).

The figure has been updated, and all the comments are considered.

Fig. 5: Why does your x-axis end at 1.4 m ice thickness? Your inversion is valid up to 1.5m thickness, so the x-axis should extent to at least 1.5 m. The same applies for Figs. 6 and 7. Why do you model incidence angles up to 60 degrees? As far as I am aware the standard “accessible” swath for all current SAR missions is 20 to 50 degrees. I suppose it doesn't hurt to include 60 degrees as well though, but be consistent in the incidence angles you include in all your figures.

The x-axis end at 1.5 m, and we now show results from 20° to 60° in Figure 1.

Fig. 6: Why have you shown only 20 and 30 degrees incidence? To save space? If you are only going to show 2 incidence angles then you should select two incidence angles that show a wider range of the standard accessible swath (e.g. 20 and 40 degrees), not two steep incidence angles as you have shown here.

Agreed. We now show results from 20° and 40°, and all the comments are considered.

Fig. 8: This figure needs to be remade. A screenshot of Google earth is not acceptable. A graticule indicating latitude and longitude, as well as a scale bar are required on a map. It would also be helpful to include an inset map indicating the study site location along Canada's east coast (i.e. include a zoomed out map with more reference features so that readers can see where Labrador is located). In the caption change “measurement site” to “study site”; change “with four Pauli RGB decompositions of Radarsat-2...” to “with Pauli RGB decompositions of the RADARSAT-2. . .”; change “induction sounder” to “EMS”. NOTE: As required by MDA's RADARSAT-2 End User License Agreement “the following copyright notice must be conspicuously displayed alongside the product”: “RADARSAT-2 Data and Products © MacDONALD, DETTWILER AND ASSOCIATES LTD. (2011) – All Rights Reserved” and “RADARSAT is an official mark of the Canadian Space Agency” must appear as a credit.

The figure has been updated, and all the comments are considered.

Fig. 11: Why 50% confidence intervals? In Fig. 10, 90% confidence intervals were used. If possible add modeled CP-Ratio vs thickness curves - it would be very interesting to see how well the model vs empirical fits agree/disagree.

Now, 90% confidence intervals were used, and the comparison between model and empirical results was presented in the text.

Fig. 12: Again the axis labels and tick labels are too small to read. Make the plot area of part (b) square to better demonstrate the strong 1:1 agreement.

The figure has been updated, and all the comments are considered.

Technical corrections

P5446, L2-7: Define all acronyms included in the abstract. Add the acronym for compact polarimetry (“CP”) on L2, add the definition for SAR on L2, and add the definition for CTRL on L7.

Done.

P5446, L9: Change “in the region of the Sea of Labrador” to “in the Labrador Sea” L17: Change “of the Arctic” to “of Arctic” L22: change “can be” to “has been”

Done.

P5447, L1: Provide the sensor name in full followed by the acronym. L2-3: change “on the ice thickness” to “on ice thickness” L20: Change “Arctic Sea” to “Arctic Ocean” L21: change “older ice” to “MYI” L22: change “In conclusion,” to “Based on the existing literature,”

Done.

P5448, L13: change “directly” to “direct”

Done.

P5449, L9, Eq. (1): The bottom left element of the scattering matrix should be S_{VH} . Also note in the text that reciprocity ($S_{HV} = S_{VH}$) is assumed. L10: Include a definition of the subscripts of the scattering matrix provided in Eq. (1). (i.e. “where S_{pq} denotes the p transmit and q received linear polarization.”). L11: change “coherence matrix” to “coherency matrix”. L18, Eq. (3): provide a reference to Nord et al (2009) for this equation.

Done.

P5450, L5: Ensure you are consistent with upper/lower case for the subscript characters in your equations - Σh should be ΣH on this line. L6: Replace Σh with ΣH (on first line in Eq. 6) L17: Change “coherence matrix” to “coherency matrix” L18: Replace Σh with ΣH (in Eq. 8)

Done.

P5451, L13 and L22: change “incident angle” to “incidence angle”.

Done.

P5452, L1: change “incident angle” to “incidence angle”. . . Check for this typo throughout the manuscript. L12: Add reference to Iodice et al. (2011) for Eq. (10).
Done.

P5453, L4: change “. . .we propose the. . .” to “. . .we propose to exploit the. . .” L4-5: change “(here called CP-Ratio)” to “(here denoted as the CP-Ratio)” L6, Eq. (11): change “Ratio =” to “CP-Ratio =” L14-15: change “. . .dielectric constant of surface...” to “. . .dielectric constant of the surface. . .”
Done.

P5454, L3: change “. . . insensitive to the surface slope variations. . .” to “. . . insensitive to surface slope variations. . .” L24: Symbols are in wrong order; change “The thickness and surface temperature . . . are T0 and H.” to “The thickness and surface temperature ... are H and T0, respectively.”
Done.

P5455, L24: add symbols for the ice-water interface temperature (T_b) and ice surface temperature (T_0) L25: Fix units for density, should be kg m^{-3} .
Done.

P5456, L11-12: Be consistent with the symbols used for ice thickness and brine volume fraction. In Tables 1 and 2 you used H and f_{vb} , yet here in the text you have used h and f_v : L19: change “. . . due to the desalination process” to “. . . due to desalination processes” L22: change “C band” to “C-band”
Done.

P5457, L1: change “. . .ice thickness < 0.4 m” to “. . . ice thickness is < 0.4 m” L2: add a reference to Cox and Weeks (1983) here. L8-9: change “. . .changes in particular. . .” to “. . .has an effect on. . .” L11: change “. . .is less reduced than. . .” to “. . .is greater than. . .” L17: add the acronym “DFO” for the department of Fisheries and Ocean Canada.
Done.

P5458, L1: change “. . .deformed ice; the maximum. . .” to “. . .deformed ice, where the maximum. . .” L2: remove “in the worst cases”. L10: Change “Radarsat-2” to RADARSAT-2” (fix this throughout the manuscript). L27: Change “in situ” to “airborne”.
Done.

P5459, L5: Change “Deformed ice, ridge, and iceberg areas” to “Regions of deformed sea ice and icebergs were removed. . .” L7: Delete “The” from the start of 4. L16: Typo “GRP” should be “GPR”, add “EMS” before snow-plus-ice thickness. L18: I think this refers to the wrong equation, should refer to Eq. (11)? L20: Remove comma after “. . . ensures that”. L25: change final sentence to “. . . and the modal thickness (peak), representing the ice thickness most frequently encountered, was 0.50 m.”

Done.

P5460, L4: change “. . .with corresponding values of CP-Ratio. . .” to “. . .against the corresponding values of the CP-Ratio. . .” L21: change “. . .the level of CP-Ratio decreases. . .” to “. . . the level of the CP-Ratio increases. . .” L24: define the acronym for correlation coefficient (CC), prior to using it in Eq. (15).

Done.

P5462, L21: change “and independent” to “and is independent”

Done.

P5463, L3: replace “matching” with “coincident”

Done.

REFERENCES: Please review your references list carefully. A few typos/errors I noticed are listed below. P5464 L18: “olarimetric” should be “polarimetric” P5465 L11: The first author “Monaco” should be “del Monaco” P5465 L19: Article title is missing “synthetic” from synthetic aperture radar.

Done.

Table 1: For the incident shortwave radiation term: Equations column, second row: Should “cosH” at the end of the equation be “cosHa”? Parameters column, third row: Should “C in the range 0 to 10” be “C in the range 0 to 1”? Parameters column, fifth row: what does d represent? I don't think it has been defined. Comments column, final line: change “Universal Time Coordinated” to “Coordinated Universal Time” For the long wave radiation term: Parameters column, bottom row: should “e is the water vapour pressure at Ta (unit: Hpa)” be moved to the comments column? Also e is not used in the equation – is this a typo? Should e replace d in the equation for the emissivity of the atmosphere? For the upward conductive heat flux term: Parameters column, equation for k: the term V_b is undefined, I assume this is a typo and should be f_{vb} ?

The table has been updated, and all the comments are considered.

Table 2: Remove “parameters” from the end of the caption. For the sea ice density and brine volume fraction equations the terms F1 and F2 are undefined. I would also suggest using T_i instead of T for the ice temperature. For the sea ice salinity equations the unit m in the thickness conditions should not be italicized.

The table has been updated, and all the comments are considered.

Fig. 1: Include the σ symbol in the x-axis label.

Done.

Fig. 2: Include the ϵ symbol in the x-axis label. Change “constants” to “constant” (singular).

Done.

Fig. 3: Change “Structure” to “Structural” in figure caption. Ensure all your subscripts are correct in the figure (e.g. the subscripts for the permittivities of ice and brine need to be reversed).

The figure has been updated, and all the comments are considered.

Fig. 6: Typo in caption “. . . for Ratio. . .” should be “. . . for CP-Ratio. . .”.

Done.

Fig. 7: Typo in caption “. . . for Ratio. . .” should be “. . . for CP-Ratio. . .”.

Done.

Fig. 10: Typo, both regression and line should be singular in the caption.

Done.

Fig. 11: Typos in caption, “incident” to “incidence”; “angle”, “fit”, “interval” and “color” all need to be pluralized.

Done.

Fig. 13: Include the σ symbol in the x-axis label. Change “correlation” to “correlation coefficient” in the caption.

Done.

Part III

To the editor and reviewer 3:

We have revised the paper to address the main issues raised by the reviewers, as well as to include minor modifications of the authors. In the following list, we first address the major issues that are of importance in general, then we refer to the issues raised by reviewer 2. The major revisions of this paper including 4 parts:

(1) We reorganized Section 1 “Introduction”. We emphasized the significance of retrieving the sea ice thickness distribution from CP SAR both in the ice services and sea ice forecasting. And an overview of the differences between dual-, quad- and compact-polarimetric modes was provided.

(2) In section 3 “Simulation”, we carefully discuss the effect of snow layer, and we used real scenario roughness parameters to evaluate the rough surface scattering contribution now.

(3) For data process in Section 4.2, the processing chains were described detailed. The procedure of ice drift correction was provided. The method of segmentation level and deformed ice was modified, the new processing chain can exclude deformed ice, and the ice thickness values > 2.2 m has been passed.

(4) The limitations (including snow layer and environment conditions) and outlook of our

method was described and discussed.

Detailed response to the reviewers' comments is below. Reviewers' comments are in italic immediately followed by our response.

General Comments

The authors present a theoretical and experimental analysis of a new CP-ratio derived from compact polarimetry data, based on simulated data using RADARSAT-2 polarimetric data. The paper is well-reasoned and the experimental evidence supports the theoretical examination. This is a significant contribution well-suited to The Cryosphere.

A general concern is that the influence of the snow cover is not taken into account for the thermodynamic and scattering models, and it is ignored in the experimental data. There are additional items that need to be addressed prior to publication; these are outlined below. In this version, we present a discussion about the influence of the snow layer both in the section describing our simulations and in the section concerning the experimental results.

Detailed comments

P5446, L9: Change "Sea of Labrador" to "Labrador Sea".

Done.

P5448, L11: The following paper (recently accepted) should be included: Geldsetzer, T., M. Arkett, T. Zagon, F. Charbonneau, J.J. Yackel and R. Scharien, (2015). All season compact-polarimetry SAR observations of sea ice. Canadian Journal of Remote Sensing.

Is now included.

P5452, L2: Is "CC" missing in Eq.9.

No, it is used for shorten the expressions for cc and c2

P5454, L20: In Figure 3, the snow cover is missing, or ignored. Please see comment for P5459, L9, below.

The issue of a snow cover is now considered in the text (see our answers below).

P5456, L14: Why is 5.3 Ghz used instead of the 5.405 Ghz of RADARSAT-2?

Done.

P5456, L28: Perhaps include the following paper to support the change near 4 cm thickness: Isleifson, D., Hwang, B., Barber, D. G., Scharien, R. K., & Shafai, L. (2010). C-band polarimetric backscattering signatures of newly formed sea ice during fall freeze-up. Geoscience and Remote Sensing, IEEE Transactions on, 48(8), 3256-3267.

We did not include this reference, since it reports on two measurements of the co-polarization correlation coefficients observed at ice thicknesses < 6cm and > 8 cm which unfortunately does not fit into the context of our analysis provided here.

P5459, L9: On first-year sea ice the snow cover (even < 20 cm) can have significant salinity (due to brine wicking), resulting in brine volumes large enough to influence backscatter (Barber and Nghiem, 1999; Galley et al., 2009). Therefore, the snow cover cannot be ignored. The snow salinity is usually greatest in the bottom 2 to 8 cm, likely

creating a dielectric interface within the snow. This should be discussed as a possible source of error with respect to GPR measurements, in that the snow thickness may be underestimated; and thus ice thickness may be overestimated. The dielectric properties of the snow will also affect refraction, which will impact the incidence angle with regards to SPM modeled values for the sea ice surface. Please comment on how the above factors may, or may not, affect the overall results.

Barber, D. G., & Nghiem, S. V. (1999). The role of snow on the thermal dependence of microwave backscatter over sea ice. Journal of Geophysical Research: Oceans (1978–2012), 104(C11), 25789-25803.

Galley, R. J., Trachtenberg, M., Langlois, A., Barber, D. G., & Shafai, L. (2009). Observations of geophysical and dielectric properties and ground penetrating radar signatures for discrimination of snow, sea ice and freshwater ice thickness. Cold Regions Science and Technology, 57(1), 29-38.

We discussed the effects of the snow cover mentioned by the reviewer at the end of Section 3.2 and included the references. In Section 4.2 we list the measured air temperatures, which are low. Considering that heavy snow falls took place shortly before the radar measurements, and that temperatures were below -7°C between snow fall and image acquisition, we assume that we can ignore any brine wicking effects. However, we do not have any information about elder snow layers.

P5460, L8: In the CIS ice charts for March 19 and 20, 2011, there is no multi-year ice in the areas covered by the RADARSAT-2 scenes. Therefore, the thicker ice measurements require additional and/or different explanations.

Because of the new processing chain and the careful separation of level and deformed ice, we did not obtain ice thickness values > 2.2 m for the profile data that passed the thresholds in the processing chain. Hence we can exclude the presence of MY ice along our profiles.

Retrieval of the thickness of undeformed sea ice from Simulated C-band compact polarimetric SAR images

X. Zhang¹, W. Dierking², J. Zhang¹, J. M. Meng¹, and H. T. Lang³

[1]{the First Institute of Oceanography, State Oceanic Administration, Qingdao, China}

[2]{Alfred Wegener Institute for Polar and Marine Research, Bremerhaven, Germany}

[3]{Beijing University of Chemical Technology, Beijing, China}

Correspondence to: X. Zhang (schuman.zhang@gmail.com)

Abstract. In this paper we introduce a parameter for the retrieval of the thickness of undeformed first-year sea ice that is specifically adapted to compact polarimetric (CP) synthetic aperture radar (SAR) images. The parameter is denoted as “CP-Ratio”. In model simulations we investigated the sensitivity of CP-Ratio to the dielectric constant, ice thickness, ice surface roughness, and radar incidence angle. From the results of the simulations we deduced optimal sea ice conditions and radar parameters for the ice thickness retrieval. C-band SAR data acquired over the Labrador Sea in circular transmit, linear receive (CTRL) mode were generated from RADARSAT-2 quad-polarization images. In comparison with results from helicopter-borne measurements we tested different empirical equations for the retrieval of ice thickness. An exponential fit between CP-Ratio and ice thickness provides the most reliable results. Based on a validation using other compact polarimetric SAR images from the same region we found a root mean square (rms) error of 12 cm and a maximum correlation coefficient of 0.93 for the retrieval procedure when applying it to level ice between 0.1 m and 1.8 m thick.

1 Introduction

Sea ice covers about one tenth of the world ocean surface and significantly affects the exchanges of momentum, heat, and mass between the sea and the atmosphere. Not only sea ice extent is a significant indicator and effective modulator of regional and global

- 带格式的: 字体颜色: 文字 1
- 带格式的: 字体颜色: 文字 1
- 删除的内容: On the basis of
- 删除的内容: CTRL
- 删除的内容: , which
- 删除的内容: Radarsat
- 删除的内容: acquired jointly
- 删除的内容: sea ice thickness
- 删除的内容: in the region of the Sea of Labrador,
- 删除的内容: thickness
- 删除的内容: 8
- 删除的内容: 92
- 删除的内容: on
- 删除的内容: of
- 删除的内容: 9
- 带格式的: 字体颜色: 文字 1
- 删除的内容: mean thickness
- 带格式的: 字体颜色: 文字 1
- 带格式的: 字体颜色: 文字 1
- 带格式的: 字体:Times New Roman, 四号, 字体颜色: 自动, (无), 字距调整 二号

climate change, but also sea ice thickness is an important parameter from a thermodynamic and kinematic perspective (Soulis et al., 1989; Kwok, 2010). The decline of sea ice extent recently observed in the Arctic, e. g. is linked with a decrease of ice thickness and increasing fractions of thin ice areas (Kwok et al., 2009). Measurements of sea ice thickness are compared with model results to control and validate the model capabilities for reproducing recent and predicting future trends of sea ice conditions in the Arctic (Laxon et al., 2013). Although sea ice thickness is only several meters at most, it forms an effective thermal insulation layer due to its high albedo and low thermal conductivity, leading to a significant reduction in the heat flux from the ocean to the atmosphere, especially in winter (Vancoppenolle et al., 2005). Besides investigations focusing on the entire Arctic or Antarctic region, other studies analyze ice thickness variations on local scales to improve regional ice thickness retrievals (e. g. Haapala et al., 2013). Operational services charged with providing sea ice maps and forecasting ice conditions for marine transportation and offshore operations need regular information about local and regional ice thickness distributions. The use of sensors providing high spatial resolutions on the order of 100 meters or better such as SAR for ice thickness retrieval is an important topic of recent research (Dierking, 2013).

Unfortunately, the sea ice thickness distribution is also one of the most difficult parameter to measure. The most direct and accurate measurement technique is in-situ drilling with an ice auger. Although it provides data with sufficient accuracy, it is time consuming and spatially limited. Therefore, this method is used mainly for calibration of other sensors or methods. To obtain ice thickness distributions at larger spatial scales, remote sensing methods are requisite tools. There are generally different strategies:

1) Measurements of ice draft using upward-looking sonar on ocean moorings or submarines (Wadhams, 1980; Behrendt et al., 2013) from which thickness is estimated based on assumptions about buoyancy, ice density, and snow load (e. g. Rothrock et al., 1999). Such data provide information about detailed temporal thickness variations (daily or even hourly) at a fixed location. An example for using in situ measurements of ice thickness from the New Arctic Program initiated by the Canadian Ice Service (CIS) starting in 2002, and sea ice draft measurements from moored ULS instruments in the Beaufort Gyre Observing System for testing a method of ice thickness retrieval from optical methods

删除的内容: by

删除的内容: sonars

删除的内容: on the ocean floor (Wadhams, 1980) or by

is provided by Wang et al. (2010).

2) Measurements of sea ice freeboard (i.e., the part of the ice above the water level) plus snow layer thickness with laser altimetry (e. g. Wadhams et al., 1992; Dierking, 1995). From such data, the average ice thickness can be estimated, or the probability density function (PDF) of ice freeboard can be converted to a PDF of ice draft. However, the estimation of ice thickness from freeboard data is less reliable than from ice draft because of a relatively stronger impact of errors in the freeboard measurements (Goebell, 2011).

3) Measuring the distance between snow surface and ice bottom with electromagnetic induction sounders (EMS) mounted on sledges, ships or helicopters/airplanes (Goebell, 2011; Haas et al., 1997; Prinsenberg et al., 2012a, 2012b). With such systems, spatial ice thickness variations measured at horizontal distances of a few 10 meters were obtained in various regions (Kovacs et al., 1987; Rossiter and Holladay, 1994; Haas et al., 2006; Hendricks et al. 2011).

Although ULS and EMS have all contributed greatly to our knowledge about ice thickness distributions on local and regional scales, such data can be obtained only at specific locations over a limited time period. Satellite remote sensing, on the other hand, is useful to monitor ice thickness variations regularly over much larger areas.

Space-borne radiometer and altimeter have been used primarily to map ice thickness, and to monitor and study their trends. In case of L-band passive microwave sensors, such as for example the Soil Moisture and Ocean Salinity mission (SMOS) radiometer, the difference between horizontally and vertically polarized emission is correlated with sea-ice thickness. The limitation of ice thickness retrieval using this type of sensor is that it is only possible for very high (almost 100%) sea ice concentration and in cold freezing conditions (Kaleschke et al., 2012; Huntemann et al., 2014). The capabilities of laser and radar altimeter systems (such as ENVISAT radar altimeter, ERS-1/2 radar altimeter, CryoSat-2 and ICESAT) for measuring ice freeboard have been extensively investigated during the last decade (e. g. Kwok and Cunningham, 2008; Kwok et al., 2009; Laxon et al., 2013). Compared with radiometers, which collect data only at a coarse spatial resolution of a few to tens of kilometers (e.g. 25 km for SSM/I 37 GHz data), the spatial resolutions of altimeter systems are higher: about 5 km for the ENVISAT radar altimeter, and 1.2 km across-track, 250 m along-track for CryoSat-2. The sea ice products derived from

删除的内容: or ships

删除的内容:). Although these methods provide data with sufficient accuracy, they are time consuming and/or have poor spatial coverage. Low-frequency

删除的内容: radiometers,

删除的内容: L-band SMOS (

删除的内容:) radiometer, receive signal contributions from larger penetration depths in sea ice and thus contain information on the ice thickness

删除的内容: 2014). However, the

radiometers and altimeters usually focus on large-scale spatial and temporal variations. While the large-scale ice thickness product is important for climate research, the support of marine navigation and offshore operations in polar areas are crucially dependent on precise and reliable sea ice thickness maps with spatial resolutions better than 1 km. Space-borne synthetic aperture radar (SAR), which operates in the microwave frequency band, provides all-weather and day-night high-resolution imagery (within a range of 1-100 m) with 1~3 days' temporal coverage. Hence, SAR is in general very useful for operational mapping tasks on regional and local spatial scales (Dierking, 2013). The disadvantage of SAR systems is that higher spatial resolutions are linked with a limited coverage between 10 and 500 km, compared for example to more than 1000 km for passive microwave radiometers. SAR measures the intensity of the radar signal backscattered from the ice surface and volume at different polarizations. The backscattered intensity depends on the dielectric constant of the ice and small-scale (mm – dm range) ice properties such as ice surface roughness and air bubble fractions and sizes. If at least two polarizations are measured simultaneously, the SAR, which is a coherent device, can also provide the phase difference between the differently polarized channels. The most recent SAR sensors have polarimetric capabilities. A fully polarimetric radar transmits and receives both linear horizontal (H) and vertical (V) polarized electromagnetic waves. Amplitude and phase information of the backscattered signal are recorded for four transmit/receive polarizations (HH, HV, VH and VV). This mode is commonly referred to as “quad-pol”. Quad-pol scenes are usually acquired at very high spatial resolution. The RADARSAT-2 scene has a spatial resolution of 4.7 m (slant range) × 5.0 m (azimuth) (at a swath width of 25/50 km). Dual-pol scenes contain two polarimetric channels (e.g. HH and HV or VV and VH). In operational ice-charting services dual-pol scenes are preferred because of their wider areal coverage, e.g. the RADARSAT-2 ScanSAR Wide mode can have a swath width of 500 km with 160-72 m (ground range) × 100 m (azimuth) resolution. Despite their currently very limited coverage, the quad-pol images are important information sources to understand the scattering mechanisms of sea ice. Recently a number of investigators noted correlations between ice thickness and the co-polarization ratio, which is the ratio of measured intensities at VV- and HH-polarization (here we use VV/HH). The sensitivity between co-polarization ratio and thin ice thickness

删除的内容: such

删除的内容: only

删除的内容: (Kwok et al., 2009), and their coarse resolution prevents the retrieval of the sea ice thickness distribution on a finer scale. This situation encouraged us to study alternative approaches to obtain sea-ice thickness distributions at much higher spatial resolution. Synthetic

删除的内容:) can provide observations all-day and at almost

删除的内容: conditions at

删除的内容: spatial

删除的内容: different mapping tasks. Recent papers have

has been firstly demonstrated by Onstott (1992), based on C-band radar data from the Eastern Arctic region. Kwok et al. (1995) estimated the thin ice thickness (0 to 0.1m) from L- and C- band fully polarimetric airborne SAR data acquired over the Beaufort Sea. Their approach included the training of a neural network. L-band polarimetric characteristics of ice in the Sea of Okhotsk were investigated by Wakabayashi et al. (2004), and the L-band co-polarized ratio was used to estimate ice thicknesses between 0 and 2 m (their Fig. 13). The investigation was further extended to other sensors, e.g. to the airborne Pi-SAR (X-, and L-band, data from the Sea of Okhotsk; Nakamura et al., 2009a; Toyota et al., 2009), and to ENVISAT ASAR, using radar intensity and ice thickness data from 0.2 to 2.5 m, the latter acquired from a research vessel in the Lützw-Holm Bay Antarctica (Nakamura et al., 2009b). The good correlations were attributed to the fact that the co-polarized ratio values are sensitive to the dielectric constants of the ice surface layer which changes due to the process of desalination during ice growth. The relationship between relatively thick multi-year ice (thickness between 2 m and 5 m), on the one hand, and co-polarized correlation and cross-polarized ratio HV/HH or VH/VV, on the other hand, was also investigated in the Arctic Ocean employing RADARSAT-2 and TERRASAR-X data (Kim et al., 2012). They found that the degree of depolarization is linked to the thickness of the MYI as ice surface roughness increases and salinity decreases. Although the above mentioned parameters derived from polarimetric SAR imagery have shown the potential for estimating sea-ice thickness under certain conditions, polarimetric SAR data can presently only be acquired at limited swath-widths. The quad-pol mode on RADARSAT-2, has a swath width of only 25-50 km, as mentioned above. The swath width of the VV/HH dual-polarization Stripmap mode on TerraSAR-X is 15 km. Therefore, they are insufficient for operational use which requires a large-scale coverage (Scheuchl et al., 2004). The limited swath-width also restricts scientific investigations to local domains. An alternative is to use compact polarimetry. The methods of generating compact polarimetric (CP) information (explained below) are based on receiving data at two different polarizations (Souvris et al., 2005; Raney, 2007). Compared with the “traditional” dual-polarization modes described above, CP data include a greater amount of polarization information (but less than quad-polarization data). They can cover much greater swath widths compared to quad-polarization modes due to reduced

删除的内容: the feasibility of retrieving ice thickness from SAR data (

删除的内容: .,

删除的内容: 2009
删除的内容: ; Liu et al., 2013; Kim et al., 2012). A number of studies have shown that the co-polarized ratio (Wakabayashi et al., 2004;

删除的内容: 2009; Toyota et al., 2009) and the alpha angle (Liu et al., 2013) reveal good correlations with the thickness of first-year level ice.
删除的内容: and the alpha

删除的内容: ice,

删除的内容: for multi-year ice (MYI) areas
删除的内容: Sea
删除的内容: It was
删除的内容: older ice
删除的内容: In conclusion, we anticipate

删除的内容: from polarimetric SAR imagery

删除的内容: is the reduced
删除的内容: width that makes those imaging modes less appropriate for routine mapping, which requires large-scale coverage. The quad-polarization
删除的内容: Radarsat
删除的内容: for example,
删除的内容: only
删除的内容: Compact

已移动(插入) [1]

删除的内容: SAR modes have

删除的内容: dual
删除的内容: modes, while covering

power consumption and data storage requirements.

The term “CP system” refers to a unique polarization in transmission and coherent dual-orthogonal polarizations in reception. There are three different CP configurations (Nord et al., 2009). The first architecture is the “ $\pi/4$ mode” with a slant linear transmission and horizontal (H) and vertical (V) receptions (Souyris et al., 2005). The second is the “dual circular (DC) mode”, i.e. transmitting at a single circular polarization and receiving two orthogonal circular polarizations. The last approach is circular transmit and linear (H and V) receive (called CTRL mode). Among these three compact polarization modes, the latter has been ranked to be the most promising in terms of performance and receiver complexity. The current Indian RISAT-1, the Japanese ALOS-2 and the planned Canadian RADARSAT Constellation Mission (RCM) also support the CTRL mode. According to the description in Geldsetzer et al. (2015), the coming CTRL mode of RCM will be particularly tailored to sea ice applications by offering a medium-resolution mode with a swath width of 350 km and a resolution of 50 m, a low-noise mode with the same swath width and a resolution of 100 m., or a low-resolution mode with a swath width of 500 km and a resolution of 100 m. Hence, the CTRL modes of RCM are well suited for operational sea ice monitoring.

However, one apparent disadvantage of the CP mode as compared to dual- or quad-polarization mode is the fact that the HH, VV, and HV signal combinations are not directly measured. This means that the co-polarized ratio (Wakabayashi et al., 2004; Nakamura et al., 2009a; Toyota et al., 2009) and the cross-polarized ratio (Kim et al., 2012) which are often used as an ice thickness proxy cannot be directly calculated from CP mode SAR data. Although CP SAR images have been used to distinguish sea ice types (Dabboor and Geldsetzer, 2014; Charbonneau et al., 2010; Geldsetzer et al., 2015), to our knowledge there have been no published studies on its use for ice-thickness detection in the open literature until now. Therefore, in this study, we considered the CTRL mode and developed an approach to directly retrieve the thickness from CP SAR data (hereafter we assume that the CP SAR is operated in CTRL mode). The paper is organized as follows: in Sect. 2 we introduce a new parameter to estimate ice-thickness and demonstrate its sensitivity to different ice parameters by numerical modeling in Sect. 3. In Sect. 4, an empirical relationship based on a comparison of CP-SAR signatures with ice thickness data obtained from electromagnetic induction sounding is presented, and the retrieval performance of this

已移动(插入) [2]

已上移 [1]: (Souyris et al., 2005; Raney, 2007).

删除的内容: Considering that CP data

删除的内容: available for swath widths

删除的内容: spatial resolutions of 50 m (Salberg et al., 2014), the application of CP is a key issue for sea ice surveillance, making it is

删除的内容: One

删除的内容: 2009

带格式的: 英语(美国)

删除的内容: in

已上移 [2]: a slant linear transmission and horizontal (H) and vertical (V) receptions (Souyris et al., 2005).

删除的内容: The second is the dual circular (DC) mode operating a single circular polarization transmission and two orthogonal circular polarizations on reception. The last approach is circular transmission and H and V receptions (called CTRL mode). Among these three compact polarization modes, the latter has been ranked to be the most promising in terms of performance and receiver complexity (Denbina and Collins, 2012; Panigrahi et al., 2012; Salberg et al., 2014). The Mini-SAR on Chandrayaan-1, the first practical radar, is based on the CTRL architecture. The current Indian RISAT-1, the Japanese ALOS-2 and the planned Canadian Radarsat Constellation Mission also support the CTRL mode (Salberg et al., 2014).

删除的内容: of undeformed first-year sea-ice

删除的内容: .

algorithm is described. Further discussions and conclusion are presented in Sect. 5.

2 Model and method

2.1 Full polarimetry and compact polarimetry

The full polarimetric radar scattering return can be represented by the scattering matrix \mathbf{S}

$$\mathbf{S} = \begin{bmatrix} S_{HH} & S_{HV} \\ S_{VH} & S_{VV} \end{bmatrix} \quad (1)$$

where S_{pq} denotes the p transmit and q received linear polarization. In the monostatic case and considering that reciprocity can be assumed for sea ice and snow, $S_{HV} = S_{VH}$. We use the coherency matrix \mathbf{T} to evaluate the second-order statistics of the scattering matrix \mathbf{S} . The coherency matrix \mathbf{T} formed from the elements of the scattering matrix \mathbf{S} is

$$\mathbf{T} = \frac{1}{2} \begin{bmatrix} \langle |S_{HH} + S_{VV}|^2 \rangle & \langle (S_{HH} + S_{VV})(S_{HH} - S_{VV})^* \rangle & 2\langle (S_{HH} + S_{VV})S_{HV}^* \rangle \\ \langle (S_{HH} - S_{VV})(S_{HH} + S_{VV})^* \rangle & \langle |S_{HH} - S_{VV}|^2 \rangle & 2\langle (S_{HH} - S_{VV})S_{HV}^* \rangle \\ 2\langle S_{HV}(S_{HH} + S_{VV})^* \rangle & 2\langle S_{HV}(S_{HH} - S_{VV})^* \rangle & 4\langle |S_{HV}|^2 \rangle \end{bmatrix} \quad (2)$$

where $*$ denotes the complex conjugate and $\langle \bullet \rangle$ the ensemble average.

Consider the CTLR mode for which the scattering vectors are given by (e. g. Nord et al, 2009)

$$\vec{k}_{CTLR} = [S_{RH} \quad S_{RV}]^T = [S_{HH} - iS_{HV} \quad -iS_{VV} + S_{HV}]^T / \sqrt{2}. \quad (3)$$

As usual, the “ R ” denotes that the transmitted polarization is right circular, while “ H ” and “ V ” stand for the linear reception. We set

$$\Sigma_H = S_{RH} + iS_{RV} \quad \Sigma_V = S_{RH} - iS_{RV}, \quad (4)$$

From Eq. (3) it then follows that

$$\Sigma_H = S_{HH} + S_{VV} \quad \Sigma_V = S_{HH} - S_{VV} - i2S_{HV}. \quad (5)$$

The terms $\langle |\Sigma_H|^2 \rangle$ and $\langle |\Sigma_V|^2 \rangle$ can be expressed as

$$\begin{aligned} \langle |\Sigma_H|^2 \rangle &= \langle (S_{HH} + S_{VV})(S_{HH} + S_{VV})^* \rangle \\ &= \langle |S_{HH} + S_{VV}|^2 \rangle, \end{aligned}$$

删除的内容: coherence

删除的内容: coherence

删除的内容: suggested by (Raney, 2007) with right circular polarization on transmission and an orthogonal combination of H and V polarizations on reception. The

删除的内容: for the CTLR mode

删除的内容: ,

$$\begin{aligned}
\langle |\Sigma_V|^2 \rangle &= \langle (S_{HH} - S_{VV} - i2S_{HV})(S_{HH} - S_{VV} - i2S_{HV})^* \rangle \\
&= \langle (S_{HH} - S_{VV})(S_{HH} - S_{VV})^* \rangle + \langle i2S_{HV}^*(S_{HH} - S_{VV}) \rangle - \langle i2S_{HV}(S_{HH} - S_{VV})^* \rangle + 4|S_{HV}|^2. \quad (6) \\
&= \langle |S_{HH} - S_{VV}|^2 \rangle + \langle i2S_{HV}^*(S_{HH} - S_{VV}) \rangle - \langle i2S_{HV}(S_{HH} - S_{VV})^* \rangle + 4|S_{HV}|^2
\end{aligned}$$

Under the assumption of reflection symmetry, the cross- and co-polarized scattering coefficients are uncorrelated. This assumption is reasonable for snow and sea ice surfaces at various frequencies and for different spatial scales (Souyris et al., 2005). Hence

$$\langle S_{HV}^* S_{VV} \rangle = \langle S_{HH} S_{HV}^* \rangle \approx 0. \quad (7)$$

and Eq. (6) can be rewritten by the elements of coherency matrix **T**:

$$\langle |\Sigma_H|^2 \rangle = \langle |S_{HH} + S_{VV}|^2 \rangle = t_{11} \quad \langle |\Sigma_V|^2 \rangle = \langle |S_{HH} - S_{VV}|^2 \rangle + 4|S_{HV}|^2 = t_{22} + t_{33}. \quad (8)$$

2.2 X-Bragg model and X-SPM model

According to the results obtained by the Cold Region Research and Engineering Laboratory (CRREL'88), the typical ranges of RMS height and correlation lengths for smooth level sea ice are 0.02~0.143 cm and 0.669~1.77 cm respectively (Fung, 1994). For C-band SAR, the small perturbation method (SPM) can be applied for explaining the surface scattering characteristics from smooth level sea ice. By doing so the underlying assumption is that the received radar signatures are typical for Bragg scattering. However the SPM fails to describe cross-polarization and de-polarization effects that are observed in real SAR data. In order to overcome these limitations and to widen the SPM range of validity, an extended Bragg model (termed X-Bragg model) was presented by Hajnsek et al. (2003). In the X-Bragg model the scattering surface is composed of rough randomly tilted facets that are large with respect to the wavelength but small with respect to the spatial resolution of the sensor (for RADARSAT-2 fine-quad mode, the wavelength is 5.6 cm and the resolution is 8 or 25 m). Scattering from each rough facet is evaluated by employing the SPM, whereby for the facets a random tilt is assumed which causes both a random variation $\Delta\theta$ of the incidence angle θ and a random rotation β of the local incidence plane around the line of sight. In the X-Bragg model, the random incidence angle variation $\Delta\theta$ is ignored, and the incidence plane angle of rotation β is assumed to be uniformly distributed in an interval $(-\beta_1, \beta_1)$, where the parameter β_1 is used to characterize the large-scale

删除的内容: coherence

删除的内容: the small perturbation method (SPM) can be applied for the typical ranges of RMS height and correlation lengths found for this type of ice.

带格式的: 英语(美国)

删除的内容:

删除的内容: usually

删除的内容: .

删除的内容: whereat

删除的内容: facet

删除的内容: incident

roughness (del Monaco et al., 2009).

In order to improve the range of validity of the X-Bragg model, different approaches (termed X-SPM model) were proposed by del Monaco et al. (2009) and Iodice et al. (2011). In those studies, more realistic distributions of β and $\Delta\theta$ were derived by assuming that the range and azimuth facet slopes are Gaussian random variables. The coherency matrix of the X-SPM model (T_{X-SPM}) after ensemble averaging over the local incidence angle θ_l and rotation angle β can be expressed as follows (del Monaco et al., 2009)

$$T_{X-SPM} = \rho \begin{bmatrix} \langle |R_S + R_P|^2 \rangle_{|\theta_l} & c_2 \langle (R_S - R_P)(R_S + R_P)^* \rangle_{|\theta_l} & 0 \\ c_2 \langle (R_S + R_P)(R_P - R_S)^* \rangle_{|\theta_l} & cc_2 \langle |R_S - R_P|^2 \rangle_{|\theta_l} & 0 \\ 0 & 0 & ss_2 \langle |R_S - R_P|^2 \rangle_{|\theta_l} \end{bmatrix}, \quad (9)$$

$$c_2 = \langle \cos 2\beta \rangle_{|\beta} = -1 + 2cc,$$

$$cc_2 = \langle \cos^2 2\beta \rangle_{|\beta} = \frac{\sin^2 \theta}{\sigma^2} + (1 - 2cc) \frac{\sin^2 \theta + \sigma^2}{\sigma^2},$$

$$cc = \langle \cos^2 \beta \rangle_{|\beta} = \sqrt{\frac{\pi \sin^2 \theta}{2\sigma^2}} \exp\left\{\frac{\sin^2 \theta}{2\sigma^2}\right\} \text{Erfc}\left\{\sqrt{\frac{\sin^2 \theta}{2\sigma^2}}\right\},$$

$$ss_2 = \langle \sin^2 2\beta \rangle_{|\beta} = 1 - cc_2.$$

Here, $\langle \cdot \rangle_{|\theta_l}$ means averaging over the local incidence angle; θ_l which is used to characterize the random slope variations of the facets; $\langle \cdot \rangle_{|\beta}$ means averaging over the rotation angle β ; ρ includes small scale roughness effects, and σ is the standard deviation of the surface slope which is a Gaussian random variable. Erfc{ \cdot } is the complementary Gauss error function. R_P and R_S are the Bragg scattering coefficients perpendicular and parallel to the incident plane, respectively. Both are functions of the complex permittivity ε and the incidence angle θ (Iodice et al., 2011)

$$R_S = \frac{\cos \theta - \sqrt{\varepsilon - \sin^2 \theta}}{\cos \theta + \sqrt{\varepsilon - \sin^2 \theta}} \quad R_P = \frac{(\varepsilon - 1) \left[\sin^2 \theta - \varepsilon (1 + \sin^2 \theta) \right]}{(\varepsilon \cos \theta + \sqrt{\varepsilon - \sin^2 \theta})^2}. \quad (10)$$

In the paper by del Monaco et al. (2009) it is demonstrated that the X-SPM model coincides with the X-Bragg model when the standard deviation of the surface slope is zero, and that the X-Bragg model can only be applied for standard deviations of the surface slope $\sigma < 0.1$. When $\sigma > 0.1$, the effects of incidence angle fluctuations, which is ignored in the X-Bragg

带格式的: 字体颜色: 文字 1

带格式的: 字体颜色: 文字 1

删除的内容: incident

域代码已更改

删除的内容: incident

model, is significant (del Monaco et al., 2009). Because of its wider range of validity, we used the X-SPM model in our study.

2.3 Inversion model

For ice thickness retrievals we propose to exploit the ratio between $\langle |\Sigma_V|^2 \rangle$ and $\langle |\Sigma_H|^2 \rangle$ (here denoted as the CP-Ratio). The CP-Ratio can be written as (see Eq. 4)

$$CP-Ratio = \frac{\langle |\Sigma_V|^2 \rangle}{\langle |\Sigma_H|^2 \rangle} = \frac{\langle |S_{RH} - iS_{RV}|^2 \rangle}{\langle |S_{RH} + iS_{RV}|^2 \rangle}. \quad (11)$$

By relating the CP-Ratio to the elements of the coherency matrix given for the X-SPM we obtain

$$CP-Ratio = \frac{\langle |\Sigma_V|^2 \rangle}{\langle |\Sigma_H|^2 \rangle} = \frac{cc_2 \langle |R_S - R_P|^2 \rangle_{|\theta_l} + ss_2 \langle |R_S - R_P|^2 \rangle_{|\theta_l}}{\langle |R_S + R_P|^2 \rangle_{|\theta_l}} \quad (12)$$

$$= \frac{\langle |R_S - R_P|^2 \rangle_{|\theta_l}}{\langle |R_S + R_P|^2 \rangle_{|\theta_l}}$$

Equation (12) shows that the CP-Ratio is controlled by ensemble averages of the difference and sum of the Bragg coefficients with respect to the incidence angle. From del Monaco et al. (2009), the probability density function for $\cos\theta_l$ is a normal distribution with mean $\cos\theta$ and standard deviation equal to $\sigma \sin\theta$. After averaging over variations of the local incidence angle θ_l , the CP-Ratio is dependent on the dielectric constant of the surface ϵ , the incidence angle θ , and the standard deviation of the surface slope σ . By using the model of del Monaco et al. (2009), the results of SAR measurements can be better explained than with the SPM.

We calculated the CP-Ratio as a function of the standard deviation of surface slope σ assuming $\epsilon=3.9+j0.15$ which are suggested in (Fung and Eom, 1982) for first year sea ice. The results show that the CP-Ratio increases with increasing standard deviation of the surface slope at fixed incidence angles and with increasing incidence angle at fixed σ (Fig. 1). The relationship between CP-Ratio and the dielectric constant is presented in Fig. 2. When the incidence angle is constant, the CP-Ratio reveals monotonically increasing

删除的内容: called

删除的内容: (Fig. 1).

删除的内容: .

values with increasing dielectric constant. [A similar trend also can be found in the co-polarization ratio \(Iodice et al., 2011\).](#)

With respect to our simulated results shown in Figs.1 and 2, it is important to note that the proposed parameter CP-Ratio is sensitive to the variation of the dielectric constant and almost insensitive to surface slope variations if $\sigma < 0.15$.

[For our analysis we use the fact that a dry snow layer is transparent at C and L frequencies \(meaning that our method is only applicable under freezing conditions\), and we do not consider metamorphosis of the basal snow layer due to brine wicking effects or due to melt-freeze cycles. We focus on undeformed Arctic young and first-year ice for which volume scattering is low because of the relatively high ice salinity, which means that the ice surface is the dominant scattering source. Then the backscattering coefficients depends on the small-scale surface roughness and the dielectric constant of the ice surface. Desalination of the ice occurs parallel to its growth due to brine drainage \(Kovacs, 1996\). The desalination process causes a decrease of the dielectric constant. Hence the basic idea of our method for retrieving ice thickness is to relate changes of the dielectric constant to ice thickness growth. Because the CP-Ratio is sensitive to the variation of the dielectric constant, it is well-suited for detecting changes of the ice thickness of smooth first-year level ice.](#)

删除的内容: the

删除的内容: . Hence it is well-suited for detecting changes of the dielectric constant of smooth first-year level ice for which Bragg surface scattering is dominant and volume scattering can be neglected in most cases

删除的内容: the

删除的内容: of sea ice. The ice salinity decreases by

删除的内容: while the ice thickness increases

删除的内容: , in turn,

删除的内容: the ice. The principle of

删除的内容: detection

3 A simulation study

3.1 Forward scattering model

In this section, we describe the combined use of an ice growth model and an electromagnetic scattering model for level sea ice to study sensitivities of *CP-Ratio* to different ice and radar properties. We applied the scattering model proposed by (Nghiem et al., 1995) to simulate the sea ice volume scattering and absorption by brine inclusions. The surface contribution was calculated with the polarimetric two-scale model (PTSM) (Iodice et al., 2011, 2013) and incoherently added to the volume term.

The sea ice scattering model configuration is presented in Fig. 3. [Note that we do not explicitly include a snow layer \(see also section 2.3\). The effects of a dry snow layer are \(1\) the dielectric contrast between ice and snow is lower than between ice and air, hence](#)

删除的内容: The

the reflectivity of the ice surface is lower; (2) the radar wavelength in the snow is shorter than in air, hence the ice surface appears rougher to the radar; (3) the incidence angle gets steeper (depending on the dielectric constant of the snow), which (relatively) causes a stronger backscattering. Since we carry out simulations with different dielectric constants (by varying temperature and brine volume fraction), surface roughness parameters, and radar incidence angles, the results obtained without snow can be transferred to cases with dry snow layers.

In our model, the uppermost layer is air with permittivity ϵ_0 , the lowermost medium is seawater with complex permittivity ϵ_2 , both enclosing the ice layer. The sea ice background is assumed to be pure ice with complex permittivity ϵ_i . The complex permittivity of brine inclusions is ϵ_b , and their fractional volume is f_b . The relative permittivity of the sea ice ϵ_{eff} is a function of the volume fraction of brine inclusions (Arcone et al., 1986; Vant et al., 1978). The ice surface roughness is described by the correlation length l , rms height s , and the standard deviation of surface slope σ . The thickness and surface temperature of the sea ice layer are H and T_0 , respectively. Lastly, the magnetic permeability of free space is μ_0 . Thickness and permittivity of sea ice are subject to dynamic changes during the ice growth process. The small-scale surface roughness (on cm-scale) may also vary temporally and spatially. This, however, can hardly be measured in the field with sufficient spatial density over larger areas. Here we do neither consider deformation processes causing surface roughness components on the order of meters. Furthermore, we assume that the scattering contribution of the ice-water interface can be neglected because of the relatively high salinity of Arctic young and first-year ice. Very thin ice for which reflections of the radar waves between surface and bottom have to be considered is excluded from this study. In our simulations, we do not take a snow cover into account. We restrict our analysis to temperatures well below freezing point, which means that a dry snow layer would change the incidence angle and the dielectric contrast at the ice surface. In case of the ice growth simulations described below, the snow has an insulating effect that changes the rate of ice thickness growth. Hence, various scenarios can be constructed, which is beyond the scope of this paper, which we regard as a first step towards developing a methodology for ice thickness retrieval using CP.

For ice growth simulations we use a 1-D thermodynamic model developed by Maykut,

删除的内容: The ice surface roughness is described by the correlation length l , rms height s , and the standard deviation of the surface slope variation σ . The thickness and surface temperature of the sea ice layer are T_0 and H .

删除的内容: change over time (e. g. frost flower growth). Here we do not consider deformation processes causing surface roughness components on the order of meters

(1978, 1982) based on the energy balance equations at the atmosphere-ocean boundary. The balance of the heat fluxes at the upper surface of the ice can be expressed as:

$$(1-\alpha)F_r - I_0 + F_L - F_E + F_S + F_e + F_C = 0. \quad (13)$$

where F_r is the incident short wave radiation, αF_r is the short wave radiation reflected by ice, and α is the albedo. I_0 is the amount of shortwave radiation absorbed in the interior of the ice layer, F_L is the incoming long wave radiation, F_E is the long wave radiation emitted by the ice, F_S is the sensible heat flux, and F_e is the latent heat flux. The last term F_C is the upward conductive heat flux, that is the heat from the bottom interface conducted through the ice to the upper surface. We assume that the temperature at the ice-water interface is at -1.8°C . The equations and parameters used in this study are listed in Table 1.

Substituting the equations and parameters listed in Table 1 into the Eq. (13) and using the Newton-Raphson iteration method, the sea ice surface temperature T_0 is obtained. Once T_0 is known, F_E , F_S , F_e and F_C can be easily calculated. A linear temperature profile within the sea ice layer is assumed. For volume scattering and absorption calculations we use a mean ice temperature (T) calculated from the melting temperature at the ice-water interface temperature ($T_b = -1.8^\circ\text{C}$) and the ice surface temperature (T_0). Furthermore, the thickness H (cm), density ρ (kg m^{-3}), brine volume fraction f_{vb} , and permittivity ϵ_{eff} of sea ice, which are directly related to the volume scattering and absorption in the ice, are obtained by the equations given in Table 2. The ice surface roughness parameters s , l and σ are set to different values considering the validity range of the X-SPM model (Ulaby et al., 1982; Monaco et al., 2009; Iodice et al., 2011).

3.2 Simulation results

To assess theoretical possibilities and limitations of ice-thickness measurements by *CP-Ratio*, we simulated the evolution of ice growth for given temperature and wind conditions based on the growth model described in Sect. 3.1. The air temperature and wind speed were set to -12°C and 10.5 m s^{-1} , respectively, throughout this simulation, based on reports from the field measurements that are described in section 4 below. The simulation started at an initial ice thickness of 1.0 cm. A finite difference scheme was used to calculate the increase of ice thickness at every 1 h step. After executing about 25 days' simulation, the following parameters were extracted as a function of time to drive the sea ice scattering model: ice

删除的内容: F_L is the incoming long wave radiation,

删除的内容: ,

删除的内容: .

删除的内容: Mg

删除的内容: f_v

删除的内容: Lastly the

删除的内容: 15

删除的内容: 23

permittivity ϵ_{eff} , thickness of ice layer H , and volume fraction of brine inclusions f_{vb} . For evaluating the rough surface scattering contribution, we took examples from roughness data presented in Onstott (1992, Table 5-3) which are given for different stages of ice growth: (1) dark nilas (thickness 5 cm) with $s=0.031$ cm and $l=1.26$ cm ($ks = 0.035$, $kl = 1.4$ for the radar frequency of 5.4 GHz, k - wavenumber), (2) light nilas (10 cm) with $s=0.12$ cm and $l=1.45$ cm ($ks = 0.14$, $kl = 1.6$), and (3) smooth first-year ice (>2 m) with $s=0.11$ cm and $l=0.54$ cm ($ks = 0.12$ and $kl = 0.6$). These values are in the validity range of the original Bragg scattering theory and should hence be fully covered by the X-SPM model presented in Iodice et al. (2011). The standard deviation of the large-scale slope σ is ranging from 0.05 up to 0.4 according to the validity range of the X-SPM model (Iodice et al., 2011).

At this point we note that a systematic relationship between small-scale surface roughness and ice thickness has never been reported. Weathering effects, melt events, and snow metamorphism influence the millimeter-to-centimeter ice surface roughness to a highly variable extent, independent of ice thickness. As we will show below, the influence of the small scale roughness on *CP-Ratio* is moderate to low, hence the issue of varying small-scale surface roughness is not very critical.

Figure 4 illustrates the simulated sea ice thickness as a function of time, and ice temperature, and volume fraction of brine inclusions as functions of ice thickness. Figure 4 clearly shows that the volume fraction of brine inclusions reduces as ice thickness increases due to desalination processes.

To investigate the dependence of *CP-Ratio* on the radar incidence angle and ice thickness, the complex scattering coefficients (S_{HH} , S_{VV} , and S_{HV}) were computed for C-band (5.4 GHz) at incidence angles of 20° - 60°. Then the *CP-Ratio* was calculated from Eq. (12). The relationship between *CP-Ratio* and sea ice thickness at case (3) (first year ice roughness conditions given above) and $\sigma = 0.1$ is shown in Fig. 5. It reveals that *CP-Ratio* exhibits a monotonically decreasing trend with growing ice-thickness at constant incidence angles. It should be noted that the sensitivity of *CP-Ratio* to vertical ice growth is much higher at smaller ice-thickness values up to approximately 0.4 m. This can be explained by fact that the ice salinity is calculated according to the relationship proposed by (Cox and Weeks, 1983). Their parameterization of salinity as a function of ice thickness reveals a

删除的内容: h

删除的内容: f_v

删除的内容: the rms height was set to

删除的内容: 9, 1.4

删除的内容: 8 mm

带格式的: 字体:非 斜体

删除的内容: , 0.15, and 0.2

删除的内容: 3 GHz), the correlation length was fixed at 18 mm ($kl = 2.0$)

删除的内容: the

删除的内容: .

删除的内容: the

删除的内容: process

删除的内容:

删除的内容: 3

删除的内容: condition $ks = 0.15$, $kl = 2.0$,

删除的内容: as discussed in Sect. 2.

带格式的: 英语(美国)

带格式的: 英语(美国)

删除的内容: between salinity

删除的内容: thickness of sea ice. When the sea

删除的内容: <

discontinuity at a thickness of 0.4 m.

Figure 6 and 7 indicate the roughness dependencies of the *CP-Ratio*. In Fig. 6 the standard deviation of surface slope σ is varied from 0.05 to 0.4 and the small-scale roughness is fixed at case 2 (light nilas) roughness condition. When σ is smaller, the effect of the variability of the ice-surface slope on the sensitivity of the *CP-Ratio* to ice thickness is small; however, at larger values of σ , this effect becomes significant and weakens the capability of *CP-Ratio* to estimate thickness. Given the same σ -values, the sensitivity of *CP* is higher at larger than at smaller incidence angles. Figure 7 reveals that the small-scale roughness has an effect on the magnitude of the *CP-Ratio* but its sensitivity to ice thickness remains on acceptable levels at higher incidence angles. At larger angles, the magnitude of *CP-Ratio* is greater than at smaller ones. From the results of these simulations, we expect that the proposed new parameter for thickness retrieval has a strong correlation with the thickness of smooth undeformed sea ice in particular at larger incidence angles, and the sensitivity is larger for thinner (<0.4 m) than for thicker sea ice. At larger incidence angles, the reduction of the radar wavelength in a snow layer on top of the ice is not a critical issue, since the effect of the small-scale roughness on *CP-Ratio* is low in this case. However, the snow layer also changes the incidence angle of the radar beam on the ice surface, which can have a considerable impact on the thickness retrieval in particular at thickness values larger than 0.3 to 0.4 m when the slope of the curves has decreased to a low value (Fig. 7). This regime, however, will not be taken for practical thickness retrievals. On first-year sea ice the bottom part of the snow layer can be saline due to brine wicking, possibly creating a dielectric interface within the snow, or resulting in brine volumes large enough to influence the radar backscatter (Barber and Nghiem, 1999; Galley et al., 2009). This may also affect the accuracy of the thickness retrieval using *CP-Ratio*.

4 Datasets and experimental results

4.1 Field Study

On 19-20 March 2011, a field program was conducted by the Department of Fisheries and Oceans Canada (DFO) along the mid-Labrador coast (Fig. 8) (Prinsenberget al., 2012a). As part of the field survey, snow thickness and ice thickness were measured with a

删除的内容: , the change of salinity is very fast, but for thickness values > 0.4 m, the process of desalination slows down

带格式的: 字体:非 斜体

删除的内容: ratio

删除的内容: the

删除的内容: parameter

删除的内容: ks- and kl-values are

删除的内容: 0.15 and

删除的内容: .0, respectively.

带格式的: 字体:非 斜体

删除的内容: < 0.15 the contribution

删除的内容: to

删除的内容: when

带格式的: 字体:非 斜体

删除的内容: > 0.15 the contribution of the ice-surface slope

删除的内容: changes in particular

删除的内容: , more or less independent of the incidence angle. At larger

删除的内容: less reduced

删除的内容: underformed

删除的内容: Canadian Ice Service (CIS) and

删除的内容: 2012). During

删除的内容: the average air temperature was around -8--12°C and the wind speed around 11~15 m s⁻¹. Snow

helicopter-borne sensor package which consists of a laser altimeter, an electromagnetic induction sounder (EMS), and a ground-penetrating radar (GPR). The laser altimeter provides the distance to the snow or ice surface, whereas the induction sounder measures the distance from the sensor to the ice-water interface. Hence the snow-plus-ice thickness can be obtained (Prinsenberget al., 2012a; 2012b). Comparisons with drill hole data showed that the ice thickness values derived from such soundings agree well within ± 0.1 m over flat homogeneous ice (Haas et al., 2006; Prinsenberget al., 2012b). The accuracy decreases over ridges and deformed ice, where the maximum thickness can be underestimated by as much as 50 % (Haas et al., 2006; Prinsenberget al., 2012b). Snow thickness profiles were collected concurrently with a ground-penetrating radar (GPR) and the laser altimeter measurements. The ground-penetrating radar which was operated at a frequency of 1 GHz, receives returns from the ice-snow and air-snow interfaces, though the return from air-snow surface is very weak. The laser altimetry is superior for defining the air-snow interface. Therefore, the combination of GPR and laser altimetry allows to retrieve the snow depth on sea ice. For a 1 GHz GPR system, the minimum detectable snow layer thickness is 0.12 m and the measurement error is 0.08 m in light dry snow. (Lalumiere, 2006) By subtracting the GPR snow thickness measurements from the EMS snow plus ice thickness measurements, sea ice thickness can be estimated.

4.2 Data sets and data processing

All data are available on the Website of DFO including pictures, notes and reports of the survey (<http://www.bio.gc.ca/science/research-recherche/ocean/ice-glace/data-donnees-eng.php>).

During the field survey, four C-band RADARSAT-2 quad-polarization images were acquired nearly coincident with the DFO airborne survey flight lines (Fig. 8). The RADARSAT-2 data were provided by the MacDonald, Dettwiler and Associates Ltd (MDA). Important SAR parameters are listed in Table 3. For our processing we used the RADARSAT-2 single-look slant range complex format as starting point. A speckle reduction filter (13x13 Lee filter) and radiometric calibration procedures were applied for the calculation of the scattering matrix. With the quad-polarization data, the CTLR compact polarimetry mode can be generated via Eq. (3). Subsequently the CP-Ratio was extracted

删除的内容: 2012

删除的内容: sounding

删除的内容: Similä

删除的内容: 2010

删除的内容: ;

删除的内容: in the worst cases

删除的内容: Similä

删除的内容: 2010

删除的内容: operating

删除的内容: 1000 MHz. Using those

删除的内容: profiles, sea ice

删除的内容: could

删除的内容: . All data are available on the DFO's Maritimes Website (<http://www.bio.gc.ca/science/research-recherche/ocean/ice-glace/data-donnees-eng.php>) including pictures, notes and reports of the survey

删除的内容: On 19

删除的内容: 20 March 2011,

删除的内容: Radarsat

删除的内容: measurement.

删除的内容: Google Earth

删除的内容: Pauli RGB images of this data set are shown in Fig. 8.

删除的内容: The Radarsat-2 data are originally processed as

删除的内容: (SSC) data in a

删除的内容: format

by Eq. (11). Lastly, the geometric registration of the simulated CP SAR images (i.e. their representation in geographical coordinates) was performed based on longitude and latitude data provided in SAR metadata.

Fig. 8 presents the ice condition at the study site, flight paths and four nearly coincident RADARSAT-2 fine quad-polarization images. Eight EMS profiles were measured within the coverage of the four SAR images, and the time differences between the SAR acquisitions and EMS flights are summarized in Table 4. The images in Fig. 8 show the RADARSAT-2 data overlain with ice thickness data collected over the fast ice and drifting pack ice. According to the ice charts, the total ice concentrations in fast-ice and pack ice regions are 10/10 and 9/10, respectively. The main ice type in land-fast is first-year ice of 70-120 cm in thickness, and the drift ice region contains grey ice (10-15 cm thick), grey-white ice (15-30 cm), thin first-year ice (30-70 cm) and again first-year ice 70-120 cm thick. In the drifting ice region several open water and scattered frazil ice areas can be seen in the SAR images. The extent of land-fast ice evolves in the offshore direction and can be visually separated from the pack ice. Most of the rougher land-fast ice is brighter in the SAR images than the thinner undeformed land-fast ice. According to the meteorological data archive from Makkovik station (<http://climate.weather.gc.ca/>), the air temperature was around -9~-17 °C on 15-16 March 2011, and heavy snow fall was registered on 17-19 March. So a large fraction of the sea ice was covered with snow, which can be clearly seen in aerial photos. On 19-20 March 2011, the average air temperature was around -8~-12°C and the wind speed around 11~15 m s⁻¹ (Prinsenberget al., 2012a). Hence the snow can be regarded as dry. We also note that thermodynamically driven effects on the bottom snow layer such as brine wicking take place at temperatures higher than -7°C (Barber and Nghiem, 1999) which means that we can ignore them here for the freshly fallen snow. However, we do not have any information about elder snow layers changed by metamorphosis processes, which may have an influence on the effective backscattering signature. Fig. 9 shows the ice thickness and snow depth profiles of the land-fast and drift ice. The histograms shown in Fig. 9 confirm that the land-fast mean ice thickness is smaller than of the drifting pack ice, and it, consists of rafted floes and reveals a deeper snow cover. The flight profiles also show that there are deformed ice or ridges (ice thickness exceeded 2.0 m) in the survey field.

已移动(插入) [3]

删除的内容: Eight EMS profiles were measured within the coverage of the four SAR images (Fig. 8). The time difference between the SAR acquisitions and EMS flights are summarized in Table 4. A direct comparison between SAR data and ice thickness may cause errors due to the time and resolution differences.

[A direct comparison between SAR imagery and flight profiles data may cause errors due to the time differences of the data acquisitions \(the time difference between SAR and flight data is shown in Table 4\). In addition, a spatial difference may be caused by the sampling and spatial resolution of the different measurement instruments.](#) The sampling rate for EMS and laser is 10 Hz, which, given typical helicopter survey speed of 80 mph, corresponds to a spatial sampling interval of about 3-4 m. While the footprint size of the laser is very small (several centimeters), the footprint of EMS is around 20 m at a typical operation height of 5-6 m. For this experiment, the GPR was configured to a scan rate of approximately 30 scans per second. When flying at 60-80 knots, the ground sample spacing is approximately one sample per 1.0-1.5 m. [Moreover, according to the DFO survey report, the floating ice drifted 1.4-1.8 knots towards southeast, as measured by ice beacons \(Prinsenberget al., 2012a\).](#) In order to mitigate the errors caused by time and spatial resolution differences, we developed the following processing chain for [Jinking SAR](#) and [airborne](#) data.

删除的内容: EM

[1. The correction of the time difference was only implemented for the drifting ice region.](#) The boundary between fast ice and drifting pack ice was taken from ice charts of the Canadian Ice Service (Fig. 8). For the eight EMS profiles, P1, P2, P5, and P7 are in or near the land-fast ice region, whereas P3, P4, P6, and P8 are from the drift ice zone. With an ice drift speed of 1.5 knots, and drift direction southeast taken from the DFO survey report and considering the respective time differences, the profiles P3, P4, P6, and P8 are shifted to the locations that should have been valid at the acquisition time of the SAR image. The shifted profiles are presented in Fig. 8 (dotted line). It should be noted that 28 hours passed between the acquisition times of the P8 and SAR data, and the new locations of P8 is beyond the coverage of the SAR image. Hence P8 was discarded from further analysis.

删除的内容: the

删除的内容: in-situ

删除的内容: 1. Open water and land regions were masked, leaving only the ice-covered region for analysis.

2. The EMS thickness values below 0.1 cm were removed to consider the measurement accuracy of the EMS. [Regions for which only EMS data but no GPR data are available were also removed.](#)

删除的内容: ice

删除的内容: .
4. The regions

删除的内容: using information in the reports, pictures and laser data that were collected along the survey lines

删除的内容: 4. The regions

[3. Regions](#) with GPR snow thickness values higher than 0.20 m were removed, because snow layers thinner than 0.20 m are nearly transparent to C-band radar waves, and the backscatter from the snow surface and volume can be neglected ([Hall et al., 2006](#)).

删除的内容: Stiles and Ulaby, 1980; Nakamura

删除的内容: 2009

[4. By combining the field survey data \(ice charts and aerial photos\), a visual interpretation of RADARSAT-2 SAR was made, and regions of open water, land, and deformed ice were](#)

删除的内容: 5. For homogeneous ice areas ("homogenous" in the sense that there is only one ice type in the area) of at least 50 m in length,

masked in the SAR images. Land was identified using the coastal line, open water areas were interpreted via backscattering and texture. Deformed ice was brighter than level ice in single-polarization SAR images, and revealed a higher entropy, which was extracted using H/A/ α decomposition (Scheuchl et al., 2002). We emphasize that in step 1 most open water areas are already excluded from further analysis.

5. For ice zones of 50 m in length, averages of different parameters were evaluated. Firstly, we used the H/A/ α unsupervised Wishart classifier to segment the SAR images, and each patch was regarded a homogeneous ice area with respect to its radar signature. Then the snow thickness, snow-plus-ice thickness, surface roughness, and simulated CP SAR data were averaged over segments of 50 m in length. Considering that the range and azimuth spacing of RADARSAT-2 fine quad-polarization are 4.7 m \times 4.9 m respectively, we applied a 13 \times 13 pixel window for the H/A/ α unsupervised classification. For the averages along transects, 13 SAR pixels, 15 EMS samples and 45 GPR samples were used.

6. Sea ice thickness was extracted from the averaged GPR snow depth and EMS snow-plus-ice thickness values.

7. Finally we calculated the CP-Ratio from equation (11) using the averaged complex backscattering coefficients.

This processing chain ensures that only level ice is considered for which the EMS system delivers reliable thickness data with an acceptable accuracy. The total length of the profile segments that we used in this study amounts to about 16 km (320 samples). Compared with the original data, almost 60% of the data were discarded in this processing chain (step 1: 17%, step 2: 10%, step 3: 23%, step 4: 10%).

4.3 Ice thickness retrieval

To investigate the possibility of using the proposed polarimetric parameter CP-Ratio to estimate sea ice thickness from SAR images, we plotted ice thickness values obtained during the field campaign described above against the corresponding values of CP-Ratio derived from the RADARSAT-2 images (all 320 samples are plotted in Fig. 10). It can be seen that at C-band, the CP-Ratio shows a negative trend relative to the ice thickness as the simulated results given in Sect. 3.2 predicted. Fig. 10 reveals that the highest sensitivity

删除的内容: along the flight transects. We used a 13 \times 13 pixel window to average scattering parameters corresponding to a fixed length of 50 m on the ground

删除的内容: GRP

删除的内容:

删除的内容: (14

删除的内容: ,

删除的内容: 10 km (702 samples). From the histograms shown in Fig. 9 we found, that the maximum ice thickness was 3.3 m, the mean ice thickness 0.91 m, and the modal thickness (peak) representing the ice thickness most frequently encountered 0.50 m.

删除的内容: with

删除的内容: Radarsat

删除的内容: As

删除的内容: ,

occurs between 0 and 0.5 m and saturates with thickness values exceeding 1.5 m. As shown in Figs. 5 to 7, the sensitivity should be smaller for ice thickness exceeding 0.4 m. However, the slope change of the curves at 0.4 m is not as abrupt as in the theoretical curves predicted in Sect. 3.2. This can be presumably explained by the fact that since we average over segments with different values of ice roughness parameters s , l and σ .

Since our data comprise different incidence angles (29°, 42° and 49° at the survey positions, Table 3), we can construct the relationships between ice-thickness and the CP-Ratio dependent on the incidence angle. We applied two different fits, a linear and a logarithmic one, to obtain an empirical relationship between the ice thickness and CP-Ratio. The best regression was obtained using a logarithmic function (Fig. 10). For Fig. 10, the empirical equations and correlation coefficients (CC) are

$$\begin{cases} \text{CP - Ratio} = 0.04935 - 0.07329 \ln(H) & \text{for } 29^\circ \text{ incident angle (CC} = 0.90) \\ \text{CP - Ratio} = 0.06345 - 0.08251 \ln(H) & \text{for } 42^\circ \text{ incident angle (CC} = 0.93) \\ \text{CP - Ratio} = 0.07744 - 0.07952 \ln(H) & \text{for } 49^\circ \text{ incident angle (CC} = 0.89) \end{cases} \quad (14)$$

where all data points (320 samples) are used to derive the empirical regressions in the thickness range from 0.1–1.8 m.

We found that the level of the CP-Ratio increases as the incidence angle increases at a given value of the sea ice thickness. This observation compares well with the forward simulation studies as shown in Fig. 5. These high correlations enable us to derive reliable thickness information for smooth level ice from radar images, assuming winter conditions (dry snow, no brine wicking). The ice thickness can be estimated using an exponential function, which can be described as follows:

$$H = \exp\left[\frac{a - (\text{CP - Ratio})}{b}\right], \quad (15)$$

where a and b are the coefficients of the exponential fit.

At the next stage, we focused on the RADARSAT-2 images #2 and #3 (which have the same incidence angle of 42°) to validate our method. Out of total 320 samples, 159 samples belong to images #2 and #3. According to the principle of independent sample test, we divided these 159 samples into two data sets. The first set includes 79 samples that are used to fit the model for estimating ice thickness, and the second one comprises 80 samples that serve to retrieve ice thickness, and compare the results with the data from the field campaign.

删除的内容: 2

删除的内容: (corresponds

删除的内容: multi-year ice). The reason is that multi-year ice survived at least one melting season so that

删除的内容: salinity is very low and almost constant in the upper ice layer, which means that the dielectric constant does not change substantially either as a function of

删除的内容: 10), which can be described as:

已上移 [3]: Fig.

删除的内容: 11). We found that the level of CP-Ratio decreases

删除的内容: For Fig. 11, the empirical equations and correlation coefficients are .

删除的内容: .

删除的内容: Radarsat

删除的内容: image

删除的内容: has

删除的内容: as image #1

删除的内容: , whereas image #1 was

删除的内容: . The resulting equation was applied to image #2

删除的内容: , which was compared

删除的内容: thickness

The coefficients a and b of the empirical fit generated from [the first data set](#) are 0.068 and 0.077 respectively. The fitted curve and validation results are presented in Fig. 11a and Fig. 11 b, respectively. The correlation coefficient for the fit shown in Fig 11a is 0.93 for the thickness range from 0.1 to 1.8 m and 0.94 for the thickness range from 0.1 to 0.6. The RMS error and the relative error between the observed and the estimated ice thickness, shown in Fig. 11b, are 12 cm and 20% in the thickness range from 0.1–1.8 m, and 8 cm and 18% for 0.1 to 0.6 m (the latter case considers the decreased sensitivity of *CP-Ratio* to larger ice thickness as discussed above). The relative RMS error implies, e.g. that the absolute RMS error is 0.2 m at an ice thickness of 1.0 m (for the range 0.1 to 1.8 m). Figure 11b also demonstrates that the error of the retrieved ice thickness is very large at values > 0.8 m which is to be expected from the theoretical curves, considering the significantly decreased sensitivity of *CP-Ratio* to larger ice thickness.

删除的内容: image #1

删除的内容: 213

删除的内容: 081

删除的内容: 12

删除的内容: were 8.05

删除的内容: 19.95

删除的内容: 5 m

带格式的: 字体: Cambria

带格式的: 缩进: 首行缩进: 0 字符

5 Discussion and conclusion

This paper provides a first analysis of sea ice thickness retrieval using compact polarimetric SAR. We developed a new parameter that we call *CP-Ratio* to estimate the thickness of undeformed first-year level ice, from C-band radar images, under dry snow conditions (snow depth < 20 cm). Numerical model simulations showed that this parameter is sensitive to changes of the dielectric constant that are linked to the growth of sea ice. We developed empirical relationships for the retrieval of level ice thickness from *CP-Ratios*. For the validation of our results we also employed [RADARSAT-2](#) images for which thickness values were available. The optimal regression between *CP-Ratio* and ice thickness was achieved with an exponential fit. The RMS error was 12 cm, and the relative error amounted to 20% for a thickness range between 0.1 and 1.8 m, and 8 cm and 18% for the range between 0.1 and 0.6 m. This indicates that the proposed parameter is very useful for the retrieval of first-year level ice thickness, even in the thickness range between 0.1 and > 1 m.

带格式的: 英语(美国)

删除的内容: .

删除的内容: obtained from polarimetric Radarsat-2 images using measured thickness data from a field campaign conducted in the Labrador Sea in 2011.

删除的内容: Radarsat

删除的内容: 8.05

删除的内容: 19.55 %.

Since the thickness of deformed ice is underestimated by the EMS measurements by as much as 50 or 60 % in the worst cases, we could only study the case of level ice. The capability of CP SAR to retrieve the thickness of deformed ice, which reveals a larger variation of large-scale roughness with respect to the sensor resolution, needs to be further

discussed and studied.

Although our tests are performed on a limited sample of images, our findings demonstrate that the C-band compact polarimetric SAR has a potential for sea-ice thickness retrievals over level first-year ice covered by a thin dry snowpack. The issue of environmental factors affecting the retrieval accuracy, e. g. brine wicking in the snow, or snow layers with different dielectric properties, has to be investigated further in more detail. The several planned Earth-observing satellite missions supporting compact polarimetry (e.g. the RCM operated at C-band) will provide the wide swath coverage necessary for operational sea ice monitoring. Hence our approach potentially provides a new operational tool for sea ice thickness measurements with a large areal coverage. In this case, the resulting thickness products are also of interest for the development, improvement, and validation of forecast models for the prediction of ice conditions, or of seasonal and climate simulations that consider Arctic and Antarctic ice conditions.

Acknowledgment

This study was supported by the National Nature Science Foundation of China under Grant 41306193, and the R&D Special Foundation for Public Welfare Industry (201305025). This work was carried out as part of the Dragon-3 Programme (10501) by the Ministry of Science and Technology of the P. R. China and the European Space Agency. The authors would like to thank the Canadian Space Agency (CSA) and MDA for providing the RADARSAT-2 data, and we are very thankful to the department of Fisheries and Oceans Canada for their support in providing valuable snow and sea ice field data. We gratefully acknowledge the detailed comments of Stefan Kern and two anonymous reviewers which helped to considerably improve the readability of the article.

References

- Arcone, A., Gow, A. G., and McGrew, S.: Structure and dielectric properties at 4.8 and 9.5 GHz of saline ice, *J. Geophys. Res.*, 91, 14281–14303, 1986.
- Barber, D. G., and Nghiem, S. V.: The role of snow on the thermal dependence of microwave backscatter over sea ice, *J. Geophys. Res.*, 104, 25789–25803, 1999.
- Behrendt, A., Dierking, W., Fahrbach, E., and Witte, H.: Sea ice draft in the Weddell Sea,

删除的内容: Sea ice deformation that results in increased surface roughness is primarily caused by compression processes. Peterson et al. (2008) and Toyota et al. (2009) have shown that the large-scale surface roughness of deformed sea ice is closely linked to the ice thickness due to ridging and rafting. Toyota et al. (2009) indicates that it may be possible to estimate the thickness distribution for deformed ice using roughness properties as proxies. Related to this suggestion, we note that the correlation coefficient between Σ_H and Σ_V could be used as a candidate parameter for determining ice-thickness with large-scale roughness. According to the X-SPM model, the correlation coefficient between Σ_H and Σ_V can be expressed as: .

删除的内容: great

删除的内容: detection.

带格式的: 缩进: 首行缩进: 0 字符

删除的内容: Radarsat

删除的内容: they

删除的内容: vey

已移动(插入) [4]

[measured by upward looking sonars, Earth Syst. Sci. Data, 5\(1\), 209-226, doi:10.5194/essd-5-209-2013, 2013.](#)

Charbonneau, F. J., Brisco, B., Raney, R. K., McNairn, H., Liu, C., Vachon, P., Vachon, W., Shang, J., DeAbreu, R., Champagne, Merzouki, A., and Geldsetzer, T.: Compact polarimetry overview and applications assessment, *Can. J. Remote Sens.*, 36, 298–315, 2010.

Cox, G. and Weeks, W.: Equations for determining the gas and brine volumes in sea-ice samples, *J. Glaciol.*, 29, 306–316, 1983.

Cox, G. and Weeks, W.: Numerical simulations of the profile properties of undeformed first-year sea ice during the growth season, *J. Geophys. Res.*, 93, 12449–12460, 1988.

Dabboor, M. and Geldsetzer, T.: Towards sea ice classification using simulated RADARSAT Constellation Mission compact polarimetric SAR imagery, *Remote Sens. Environ.*, 140, 189–195, 2014.

[del Monaco, F. D., Quattro, N. D., Iodic, A., and Natale, A.: Extended small perturbation method and retrieval of natural surface parameters, in: Proc. 6th Eur. Radar Conf., Rome, Italy, 537–540, 2009.](#)

[Dierking, W.: Laser profiling of the ice surface topography during the Winter Weddell Gyre Study 1992, J. Geophys. Res., 100, 4807–4820, 1995.](#)

[Dierking, W.: Sea ice monitoring by synthetic aperture radar, Oceanography, 26, 100–111, doi: 10.5670/oceanog.2013.33, 2013.](#)

Fukusako, S.: Thermophysical properties of ice, snow, and sea ice, *Int. J. Thermophys.*, 11, 353–372, 1990.

[Fung, A. K. and Eom, H. J.: Application of a combined rough surface and volume scattering theory to sea ice and snow backscatter, IEEE T. Geosci. Remote Sens., GE-20, 528–536, 1982.](#)

[Fung, A. K.: Microwave Scattering and Emission Models and Their Applications. Artech House, Boston, London, 1994.](#)

[Galley, R. J., Trachtenberg, M., Langlois, A., Barber, D. G., and Shafai, L.: Observations of geophysical and dielectric properties and ground penetrating radar signatures for discrimination of snow, sea ice and freshwater ice thickness. Cold Reg. Sci. Technol., 57, 29-38. 2009.](#)

已移动(插入) [5]

删除的内容: Denbina, M. and Collins, M.

已移动(插入) [6]

删除的内容: Iceberg detection using compact polarimetric

删除的内容: Atmos. Ocean, 50, 437–446, 2012

已移动(插入) [7]

已移动(插入) [8]

已移动(插入) [9]

已移动(插入) [10]

[Geldsetzer, T., Arkett, M., Zagon, T., Charbonneau, F., Yackel, J. J., and Scharien, R.: All season compact-polarimetry SAR observations of sea ice, Canadian J. of Remote Sens., doi: 10.1080/07038992.2015.1120661, 2015.](#)

Goebell, S.: Comparison of coincident snow-freeboard and sea ice thickness profiles derived from helicopter-borne laser altimetry and electromagnetic induction sounding, J. Geophys. Res., 116, C08018, doi:10.1029/2009JC006055, 2011.

[Haapala, J., Lensu, M., Dumont, M., Renner, A. H. H., Granskog, M. A., and Gerland, S.: Small-scale horizontal variability of snow, sea-ice thickness and freeboard in the first-year ice region north of Svalbard, Ann. Glaciol., 54, doi: 10.3189/2013AoG62A157, 2013.](#)

Haas, C., Gerland, S., Eicken, H., and Miller, H.: Comparison of sea-ice thickness measurements under summer and winter conditions in the Arctic using a small electromagnetic induction device, Geophysics, 62, 749–757, 1997.

Haas, C., Hendricks, S., and Doble, M.: Comparison of the sea ice thickness distribution in the Lincoln Sea and adjacent Arctic Ocean in 2004 and 2005, Ann. Glaciol., 44, 247–252, 2006.

Hajnsek, I., Pottier, E., and Cloude, S. R.: Inversion of surface parameters from polarimetric SAR, IEEE T. Geosci. Remote Sens., 41, 727–744, 2003.

[Hall, D. K., Kelly, R. E., Foster, J. L., and Chang, A. T.: Estimation of Snow Extent and Snow Properties. Encyclopedia of Hydrological Sciences, 5-55, 2006.](#)

[Hendricks, S., Gerland, S., Smedsrud, L.H., Hass, C., Pfaffhuber, A., and Nilsen, F.: Sea-ice thickness variability in Storfjorden, Svalbard, Ann. Glaciol., 52, 61-68, 2011.](#)

Huntemann, M., Heygster, G., Kaleschke, L., Krumpfen, T., Mäkynen, M., and Drusch, M.: Empirical sea ice thickness retrieval during the freeze-up period from SMOS high incident angle observations, The Cryosphere, 8, 439–451, doi:10.5194/tc-8-439-2014, 2014.

Iodice, A., Natale, A., and Riccio, D.: Polarimetric two-scale model for soil moisture retrieval via dual-Pol HH-VV SAR data, IEEE J. Sel. Top. Appl., 6, 1163–1171, 2013.

[Iodice, A., Natale, A., and Riccio, D.: Retrieval of soil surface parameters via a polarimetric two-scale model, IEEE T. Geosci. Remote Sens., 49, 2531–2547, 2011.](#)

删除的内容: .

已移动(插入) [11]

已下移 [12]: Retrieval of soil surface parameters via a polarimetric two-scale model, IEEE T. Geosci.

删除的内容: Remote,

已下移 [13]: 49, 2531–2547, 2011. .

已下移 [14]: Iodice, A., Natale, A., and Riccio, D.

已移动(插入) [14]

已移动(插入) [12]

已移动(插入) [13]

Ji, S. Y., Yue, Q. J., and Zhang, X.: Thermodynamic analysis during sea ice growth in the Liaodong Bay, *Mar. Environ. Sci.*, 19, 35–39, 2000.

Kaleschke, L., Tian-Kunze, X., Maaß, N., Mäkynen, M., and Drusch, M.: Sea ice thickness retrieval from SMOS brightness temperatures during the Arctic freeze-up period, *Geophys. Res. Lett.*, 39, 1–5, doi: 10.1029/2012GL050916, 2012.

Kim, J. W., Kim, D. J., and Hwang, B. J.: Characterization of Arctic sea ice thickness using high-resolution spaceborne polarimetric SAR data, *IEEE T. Geosci. Remote Sens.*, 50, 13–22, 2012.

[Kovacs, A., Valleau, N. C., and Holladay, J. S.: Airborne electro-magnetic sounding of sea ice thickness and sub-ice bathymetry, *Cold Reg. Sci. Technol.*, 14, 289–311, 1987.](#)

Kovacs, A.: Sea Ice, Part I.: Bulk Salinity versus Ice Floe Thickness, USA Cold Regions Research and Engineering Laboratory, CRREL Rep. 97, United States Army, Corps of Engineers, 1–16, 1996.

Kwok, R., and Cunningham, G. F.: ICESat over Arctic sea ice: Estimation of snow depth and ice thickness, *J. Geophys. Res.*, 113, C08010, doi: 10.1029/2008JC004753, 2008.

[Kwok, R., Cunningham, G. F., Wensnahan, M., Rigor, I., Zwally, H. J., and Yi, D.:](#) Thinning and volume loss of the Arctic Ocean sea ice cover: 2003–2008, *J. Geophys. Res.*, 114, C07005, doi: 10.1029/2009JC005312, 2009.

[Kwok, R., Nghiem, S. V., Yueh, S. H., and Huynh, D. D.: Retrieval of thin ice thickness from multifrequency polarimetric SAR data, *Remote Sens. Environ.*, 51, 361–374, 1995.](#)

[Kwok, R.:](#) Satellite remote sensing of sea ice thickness and kinematics: a review, *J. Glaciol.*, 56, 1129–1140, 2010.

[Lalumiere, L.:](#) Ground penetrating radar of helicopter snow and ice surveys, *Can. Tech. Rep. Hydrogr. Ocean Sci.*, 248, 1–50, http://publications.gc.ca/collections/collection_2015/mpo-dfo/Fs97-18-248-eng.pdf, 2006.

[Laxon, S. W., Giles, K. A., Ridout, A. L., Wingham, D. J., Willatt, R., Cullen, R., Kwok, R., Schweiger, A., Zhang J., Haas, C., Hendricks, S., Krishfield, R., Kurtz, N., Farrell, S. and Davidson, M.:](#) CryoSat-2 estimates of Arctic sea ice thickness and volume,

删除的内容: ,

删除的内容: Liu, M., Dai, Y., Zhang, J., Zhang, X

已上移 [7]: J.:

删除的内容: Meng,

删除的内容: Characterization

删除的内容: level sea-

删除的内容: in the Labrador Sea using C-band

删除的内容: in: IET International Radar Conference 2013, Xi'an, China, 296–296

[Geophys. Res. Lett.](#), 40, 732–737, doi: 10.1002/grl.50193, 2013.

Maykut, G. A.: Energy exchange over young sea ice in the central Arctic, *J. Geophys. Res.*, 83, 3646–3658, 1978.

Maykut, G. A.: Large-scale heat exchange and ice production in the central Arctic, *J. Geophys. Res.*, 87, 7991–7984, 1982.

[Nakamura, K., Wakabayashi, H., Naoki, K., Nishio, F., Moriyama, T., and Uratsuka, S.:](#) Observation of sea-ice thickness in the sea of Okhotsk by using dual-frequency and fully polarimetric airborne SAR (Pi-SAR) data, *IEEE T. Geosci. Remote Sens.*, 43, 2460–2469, 2009a.

[Nakamura, K., Wakabayashi, H., Uto, S., Ushio, S., and Nishio, F.:](#) Observation of sea-ice thickness using ENVISAT data from Lützw- Holm Bay, East Antarctica, *IEEE Geosci. Remote Sens. Lett.*, 6, 277–281, 2009b

Nghiem, S. V., Kwok, R., Yueh, S. H., and Drinkwater, M. R.: Polarimetric signatures of sea ice, theoretical model, *J. Geophys. Res.*, 100, 13665–13679, 1995.

Nord, M. E., Ainsworth, T. L., Lee, J. S., and Stacy, N. J. S.: Comparison of compact polarimetric synthetic aperture radar modes, *IEEE T. Geosci. Remote Sens.*, 47, 174–188, 2009.

[Onstott, R.:](#) SAR and scatterometer signatures of sea ice, in *Microwave Remote Sensing of Sea Ice, Geophysical Mono. 68, Carsey, F., Ed., Washington, DC: Amer. Geophys. Union, pp. 73–104, 1992.*

Prinsenber, S. J., Peterson, I. K., Holladay, J. S., and Lalumiere, L.: Labrador shelf pack ice and iceberg survey, March 2011, *Can. Tech. Rep. Hydrogr. Ocean Sci.*, 275, 1–44, <http://www.ocean-sci.net/275/1/2012/>, 2012a.

[Prinsenber, S., Holladay S., and Lee J.:](#) Measuring ice thickness with EISflow, a fixed-mounted helicopter electromagnetic-laser system, *Proc. 12th International Off-shore and Polar Engineering Conference, Kitakyushu, Japan, 737-740, 2012b.*

Raney, R.: Hybrid polarity SAR architecture, *IEEE T. Geosci. Remote Sens.*, 45, 3397–3404, 2007.

[Rossiter, J. R., and Holladay, J. S.:](#) Ice-thickness measurement, in *Remote Sensing of Sea Ice and Icebergs*, edited by Haykin, S. et al., pp. 141–176, John Wiley, Hoboken, N. J., 1994.

已上移 [5]: Monaco, F. D., Quattro, N. D., Iodic, A., and Natale, A.: Extended small perturbation method and retrieval of natural surface parameters, in: *Proc. 6th Eur. Radar Conf.*, Rome, Italy, 537–540, 2009.

删除的内容: .

删除的内容: .

删除的内容: 2009.

删除的内容: .

删除的内容: Mishra, A.

已上移 [10]: K.:

删除的内容: Comparison of hybrid-Pol with quad-Pol scheme based on polarimetric information content, *Int. J.*

已上移 [9]: *Remote Sens.*,

删除的内容: Panigrahi

删除的内容: 33, 3531–3541, 2012. ... 3

已上移 [11]: . K.,

删除的内容: . K.

删除的内容: Prinsenber, S. J., and Holladay, J. S.: Observations

删除的内容: thickness, surface roughness and ice motion

删除的内容: Amundsen Gulf, J.

已上移 [4]: *Res.*,

删除的内容: 113, 1–14, 2008

删除的内容: 2012,

带格式的: 字体: Cambria

删除的内容: .

删除的内容: .

删除的内容: Salberg, A. B., Rudjord, O., and Solberg, A. H. S.: Oil spill detection in hybrid-polarimetric SAR images, *IEEE T.*

[Rothrock, D. A., Yu, Y., and Maykut, G. A.: Thinning of the Arctic sea-ice cover, Geophys. Res. Lett., 26, 3469–3472, doi: 10.1029/1999GL010863, 1999.](#)

[Scheuchl, B., Flett, D., Caves, R., and Cumming, I.: Potential of RADARSAT-2 data for operational sea ice monitoring, Canadian J. of Remote Sens., 30, 448-461, 2004.](#)

[Scheuchl, B., Hajnsek, I., and Cumming, I.: Sea ice classification using multi-frequency polarimetric SAR data, in: Geosci. Remote Sens. Symposium, IGARSS'02, Toronto, Canada, 1914-1916, 2002.](#)

Soulis, E. D., Lennox, W. C., and Sykes, J. F.: Estimation of the thickness of undeformed first year ice using radar backscatter, in: [Geosci. Remote Sens. Symposium, IGARSS'89, Vancouver, Canada, 2366–2369, 1989.](#)

Souyris, J. C., Imbo, P., Fjortoft, R., Mingot, S., and Lee, J. S.: Compact polarimetry based on symmetry properties of geophysical media: The $\pi/4$ mode, IEEE T. Geosci. Remote Sens., 43, 634–646, 2005.

Toyota, T., Nakamura, K., Uto, S., Ohshima, K. I., and Ebuchi, N.: Retrieval of sea ice thickness distribution in the seasonal ice zone from airborne L-band SAR, Int. J. Remote Sens., 30, 3171–3189, 2009.

Ulaby, F. T., Moore, R. K., and Fung, A. K.: Microwave Remote Sensing: Active and Passive, vols. II, Addison-Wesley, Reading, MA, 1982.

Vancoppenolle, M., Fichefet, T., and Bitz, C. M.: On the sensitivity of undeformed Arctic sea ice to its vertical salinity profile, Geophys. Res. Lett., 32, L16502, doi:10.1029/2005GL023427, 2005.

Vant, M. R., Ramseier, R. O., and Makios, V.: The complex dielectric constant of sea ice at frequencies in the range 0.1 to 40 GHz, J. Appl. Phys., 49, 1264–1280, 1978.

[Wadhams, P., Tucker III, W. B., Krabill, W. B., Swift, R. N., Comiso, J. C., and Davis, N. R.: Relationship between sea ice freeboard and draft in the Arctic Basin, and implications for ice thickness monitoring, J. Geophys. Res., 97, 20325–20334, doi: 10.1029/92JC02014, 1992.](#)

[Wadhams, P.:](#) A comparison of sonar and laser profiles along corresponding tracks in the Arctic Ocean, in: Sea Ice Processes and Models, edited by: Pritchard, R. S., Univ. of Washington Press, Seattle, Wash., 283–299, 1980.

Wakabayashi, H., Matsuoka, T., and Nakamura, K.: Polarimetric characteristics of sea ice

已上移 [8]: Geosci.

删除的内容: Remote, 52, 6521–6533, 2014. ... [4]

删除的内容: 3-D laser scanner statistics for

删除的内容: Baltic Sea

删除的内容: , J.

删除的内容: , 115, 1–18

删除的内容: 2009JC005970, 2010

删除的内容: Geoscience and

删除的内容: Sensing

删除的内容: , 12th Canadian Symposium on Remote Sensing

删除的内容: ,

删除的内容: ... [5]

已上移 [6]: Geophys. Res.,

删除的内容: 85, 1037–1044, 1980.

in the Sea of Okhotsk observed by airborne L-band SAR, IEEE T. Geosci. Remote Sens., 42, 2412–2425, 2004.

Wang, X., Key, J. R., and Liu, Y.: A thermodynamic model for estimating sea and lake ice thickness with optical satellite data, J. Geophys. Res., 115, C12035, doi: 10.1029/2009JC005857, 2010.

Yue, Q. J., Ji, S. Y., Miao, W. D., and Wu, S. L.: Solar radiation on sea ice in Liaodong Bay, Oceanol. ET Limnol. Sin., 31, 562–567, 2000.

Table 1. Equations and parameters used for the sea ice thermodynamic model

Term	Equations	Parameters	Comments
The incident short wave radiation	$F_i = (1 - 0.0065C^2)Q_{so}a^m$ (Ji et al., 2000; Yue et al., 2000)	$a^m = 0.99 - 0.17m$	a^m is the atmospheric transmissivity;
		$m = 0.83$	C is the cloud coverage;
		C in the range 0–1	Q_{so} is the solar irradiance for the D^{th} day in a year;
		$Q_s = I_s(1 + 0.033\cos(2\pi D/365))$	I_s is the solar radiation constant (unit: W/m^2);
The long wave radiation	$F_L = (1 + kC^2)\epsilon_a\sigma T_a^4$ (Maykut, 1978)	$\delta = 23.44^\circ\cos[(172 - D)2\pi/365]$	δ is the declination angle of the sun; H_a is the local solar hour angle; β and λ are the latitude and longitude; t is
		$H_a = 15(t - 12)\pi/180 + \lambda$	Coordinated Universal Time,
		$\sigma = 5.670 \times 10^{-8}$	σ is the Stefan-Boltzman constant (unit: $\text{w}/(\text{m}^2\text{K}^4)$);
		$\epsilon_i = 0.97$	T_0 is the surface temperature of sea ice (unit: K);
The sensible heat flux	$F_s = \rho_a C_p C_s u (T_a - T_0)$ (Cox and Weeks, 1988)	$k = 0.0017$	T_a is the air temperature (unit: K);
		$\epsilon_a = 0.55 + e \times 0.052^{1/2}$	ϵ_i is the emissivity of sea ice;
		$\rho_a = 1.3$	ϵ_a is the emissivity of atmosphere;
		$C_p = 1006$	e is the water vapor pressure at T_a (unit: hPa).
		$C_s = 0.003$	C_s is the sensible heat transfer coefficient;
			u is the wind speed;

删除的内容: ,

带格式的: 字体: Cambria

带格式的: 缩进: 左: 0 cm, 首行缩进: 0 字符

删除的内容: ,

删除的内容: 10

带格式的: 下标

删除的内容: cosH

删除的内容: d

带格式的: 下标

删除的内容: Coordinated

删除的内容:

删除的内容: d

删除的内容: hPa

删除的内容:

	$F_c = \rho_a L C_e u (q_a - q_0)$ (Cox and Weeks, 1988)	$C_e = 0.00175$ $L = 2.5 \times 10^6 -$ $2.274 \times 10^3 (T_a -$ $273.15)$	L is the latent heat of vaporization (unit: J/kg);
The latent heat flux	$q_a - q_0 = \frac{0.622}{p_0} \cdot$ $\left[a(fT_a^4 - T_0^4) + b(fT_a^3 - T_0^3) + \right.$ $\left. c(fT_a^2 - T_0^2) + d(fT_a - T_0) + \right.$ $\left. e(f-1) \right]$ (Cox and Weeks, 1988)	$p_0 = 1013$ $a = 2.7798202 \times 10^{-6}$ $b = -2.6913393 \times 10^{-3}$ $c = 0.97920849; d = -$ 158.63779 $e = 9653.1925;$	p_0 is the surface atmospheric pressure (unit: mbar); f is the relative humidity; $a, b, c, d,$ and e are constants; a (unit: k^4), b (unit: k^3), c (unit: k^2), d (unit: k)
The albedo of sea ice	$\alpha = \beta_0 + \beta_1 H + \beta_2 H^2 + \beta_3 H^3$ (Cox and Weeks, 1988)	$\beta_0 = 0.2386;$ $\beta_1 = 6.015 \times 10^{-3}$ $\beta_2 = -4.882 \times 10^{-5};$ $\beta_3 = 1.267 \times 10^{-7}$	H is the sea ice thickness (unit: cm).
The absorbed shortwave radiation	$I_0 = i_0 (1 - \alpha) F_r$ (Maykut, 1978; Cox and Weeks, 1988)	$i_0 = 17\%$	i_0 is the percent.
The upward conductive heat flux	$F_c = (k/H)(T_b - T_0)$ (Cox and Weeks, 1988)	$k = k_i (1 - f_{vb}) + k_b f_{vb}$ $k_i = 4.17 \times 10^{-4} [5.35 \times$ $10^{-3} - 2.568 \times 10^{-5} (T_0 -$ $273.15)]$ $k_b = 4.17 \times 10^{-4} [1.25 \times$ $10^{-3} + 3.0 \times 10^{-5} (T_0 -$ $273.15) + 1.4 \times 10^{-7}$ $(T_0 - 273.15)^2]$ $T_b = -1.8$	k, k_i, k_b are the conductivity of ice layer, pure ice and pure brine, respectively (unit: W/m/K); T_b is the freezing point at 35 salinity (unit: °C); f_{vb} is volume fraction of sea ice brine inclusion.

删除的内容:

删除的内容:

删除的内容: f_b

Table 2. Equations and parameters used for the sea ice properties.

删除的内容: parameters

Term	Equations	Parameters	Comments
The ice thickness s	$\frac{\Delta h}{\Delta t} = \frac{F_c(H)}{\rho L_f}$ (Cox and Weeks, 1988) $H = \sum_{i=0}^{Time} \frac{\Delta h}{\Delta t} \Delta Time$	$L_f = 4.187 \times 10^3 (79.68$ $- 0.505 T_b -$ $0.0273 S_i) + 4.3115 S_i /$ $T_b + 8 \times 10^{-4} T_b S_i -$ $0.009 (T_b)^2$ (Fukusako, 1990)	$\frac{\Delta h}{\Delta t}$ is the sea ice growth rate when ice thickness is H (unit: m/s); Ice thickness is the sum of ice growth rate. $\Delta Time$ is the time lag (unit: hour).

删除的内容: $\frac{\Delta h}{\Delta t}$

域代码已更改

The sea ice density and brine volume fraction (Cox and Weeks, 1983)	$\rho = \frac{\rho_i F_1(T_i)}{F_1(T_i) - \rho_i S_i F_2(T_i)}$ $f_{vb} = \frac{\rho_i S_i}{F_1(T_i) - \rho_i S_i F_2(T_i)}$	$\rho_i = 0.917 - 1.403 \times 10^{-4} T_i$ ρ is sea ice density (unit: kg/m^3); f_{vb} is the relative brine volume fraction ρ_i is pure ice density (unit: kg/m^3); T_i is the temperature of sea ice (unit: $^{\circ}\text{C}$); T_a is the air temperature (unit: K); S_i is ice salinity. The functional forms of F_1 and F_2 can be found from the work of Cox and Weeks (1983).
The ice salinity (Cox and Weeks, 1983)	$S_i = 14.24 - 19.39H \quad (H \leq 0.4 \text{ m})$ $S_i = 7.88 - 1.59H \quad (H > 0.4 \text{ m})$	H is the ice thickness (unit: m).
The permittivity of sea ice at C-band (Arcone et al., 1986; Vant et al., 1978)	$\epsilon'_{eff} = 3.05 + 0.0072 f_{vb}$ $\epsilon''_{eff} = 0.02 + 0.0033 f_{vb}$	f_{vb} is the relative brine volume fraction.

Table 3. Specifications of [the qual-pol RADARSAT-2 SAR data](#)

Scene ID	Date/Time (UTC)	Resolution (m)*	Incidence angle (Deg.)	Beam Mode
		Rng × Az		
#1	19 Mar 2011, 10:25	5.2 × 7.7	29.0	FQ9
#2	19 Mar 2011, 21:51	5.2 × 7.7	42.0	FQ23
#3	19 Mar 2011, 21:51	5.2 × 7.7	42.0	FQ23
#4	20 Mar 2011, 09:56	5.2 × 7.7	49.0	FQ31

*Resolution is nominal. Ground range resolution varies with incidence angle.

Table 4. Specifications of helicopter-borne [EMS](#) ice thickness data sets

EM ID	SAR Scene ID coincident with EMS	Date/Time (UTC)	Time difference
P-1	#1	19 Mar 2011, 17:00-17:20	~7 hour

- 删除的内容: T
- 删除的内容: $4T$
- 带格式的: 字体:五号
- 带格式的: 字体:斜体
- 删除的内容: Radarsat
- 删除的内容: Polarization
- 删除的单元格
- 删除的内容: Resolutions...resolution (m) ... [6]
- 删除的内容: Data
- 带格式的: 居中
- 带格式表格
- 删除的内容: Incident...ncidence angle [7]
- 带格式的: 居中
- 删除的内容:
- 删除的内容: 8
- 删除的单元格
- 删除的内容: -03-19, 21:51
- 删除的内容: HH/VV/HV/VH (Quad)
- 删除的内容: 42
- 删除的内容: FQ23
- 删除的内容: 8
- 删除的内容: -03-19
- 删除的内容: HH/VV/HV/VH (Quad)
- 删除的内容: 8
- 删除的内容: -03-20, 09:56
- 删除的内容: HH/VV/HV/VH (Quad)
- 删除的内容: 49
- 删除的内容: FQ31
- 删除的内容: 8
- 删除的内容: -03-19, 10: 25
- 删除的内容: HH/VV/HV/VH (Quad)
- 删除的内容: 29
- 删除的内容: FQ9
- 删除的内容:
- 删除的内容: EM
- 带格式的: 居中, 空格 段前: 0 磅, 行距: 单线
- 删除的内容: data...cene ID coincident with EM ... [8]
- 带格式的: 空格 段前: 0 磅, 行距: 单线
- 带格式表格
- 删除的内容: Data
- 带格式的: 空格 段前: 0 磅, 行距: 单线
- 删除的内容:
- 删除的内容: -03-19
- 删除的内容: 14: 47-15

P-2	#2	19 Mar 2011 17: 25-17: 30	~4 hour
P-3	#2	19 Mar 2011 18: 30-18: 45	~3.3 hour
P-4	#3	19 Mar 2011 18: 40-18: 50	~3 hour
P-5	#4	20 Mar 2011 11: 55-12: 05	~2 hour
P-6	#4	20 Mar 2011 12: 10-12: 25	~2.5 hour
P-7	#1	20 Mar 2011 14: 25-14: 30	~28 hour
P-8	#1	20 Mar 2011 14: 40-14: 50	~28 hour

- 删除的内容: -03-19
- 删除的内容: 1
- 删除的内容: 5
- 删除的内容: 16: 00-16: 15
- 删除的内容: -03-19
- 删除的内容: 5
- 删除的内容: 16: 15-16
- 删除的内容: -03-20
- 删除的内容: < 0.5
- 删除的内容: 9: 30-9: 42
- 删除的内容: -03-20
- 删除的内容: 3
- 删除的内容: < 0.5
- 删除的内容: 9: 42-10: 00
- 删除的内容: -03-19
- 删除的内容: 4
- 删除的内容: 14: 30-14: 45
- 删除的内容: 2012-03-
- 删除的内容: 4
- 删除的内容: 26
- 删除的内容: 12: 00-12: 15
- 删除的内容: 2012-03-
- 删除的内容: 4
- 删除的内容: 26
- 删除的内容: 12: 15-12: 30

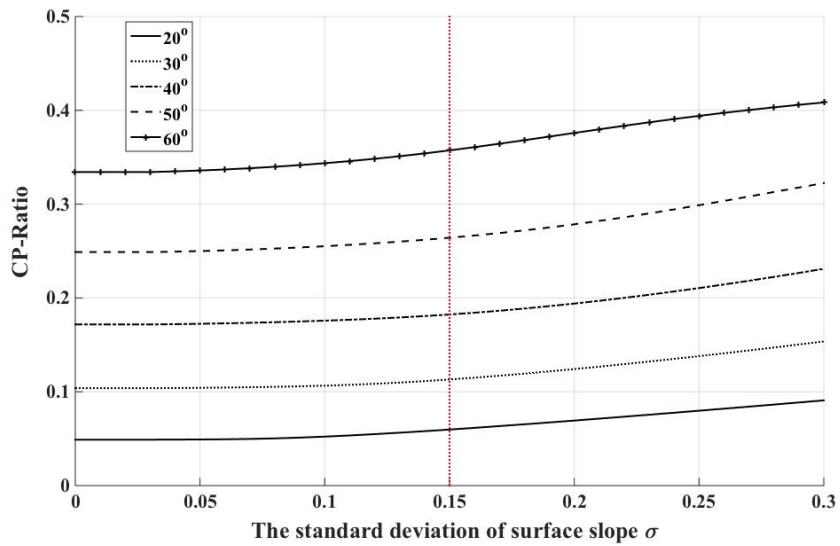


Figure 1. Variations of CP-Ratio as a function of the standard deviation of surface slope σ for different incidence angles and $\epsilon=3.9+j0.15$. The red line marks the maximum threshold of σ for the validity of our approach.

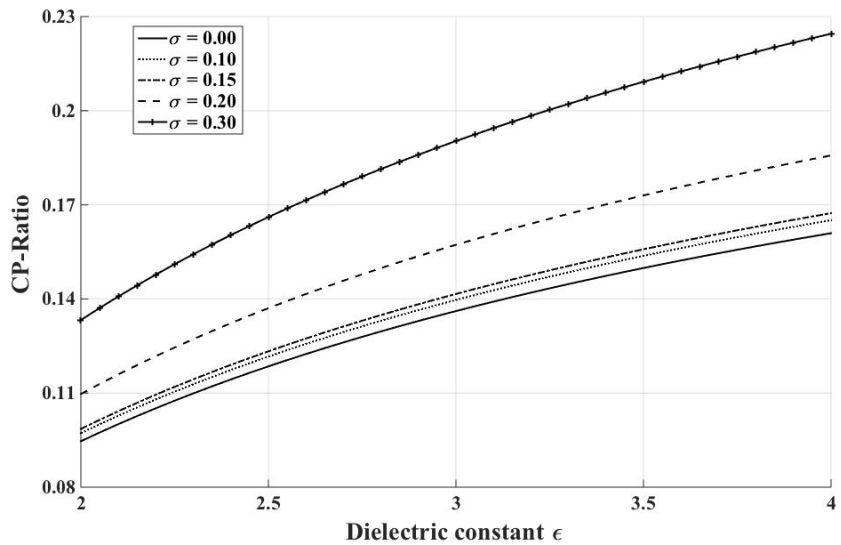


Figure 2. CP-Ratio as a function of dielectric constants for different σ and incidence angle=30°. [The results for other incidence angles follow the similar trends.](#)

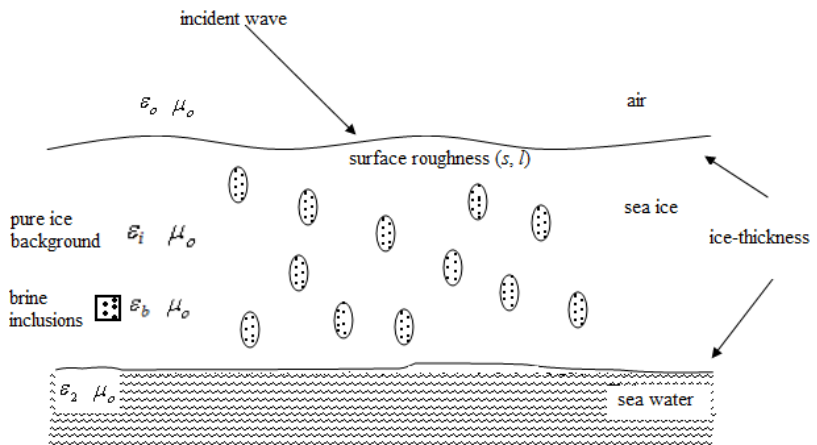


Figure 3. Structure and geometric model of the configuration of sea ice.

带格式的: 字体颜色: 自动
带格式的: 左对齐, 缩进: 首行缩进: 0 字符, 行距: 1.5 倍行距

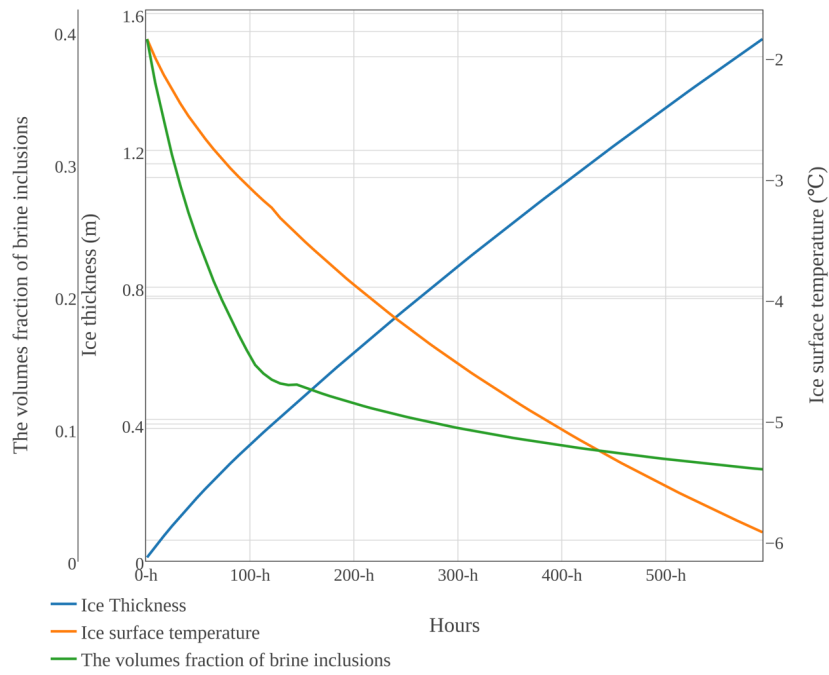


Figure 4. The simulated sea ice growth process. **Blue:** sea ice thickness; **red:** sea ice surface temperature; **green:** the volume fraction of brine inclusions.

删除的内容: (a)
 删除的内容: ,(b)
 删除的内容: ,(c)
 带格式的: 字体颜色: 自动

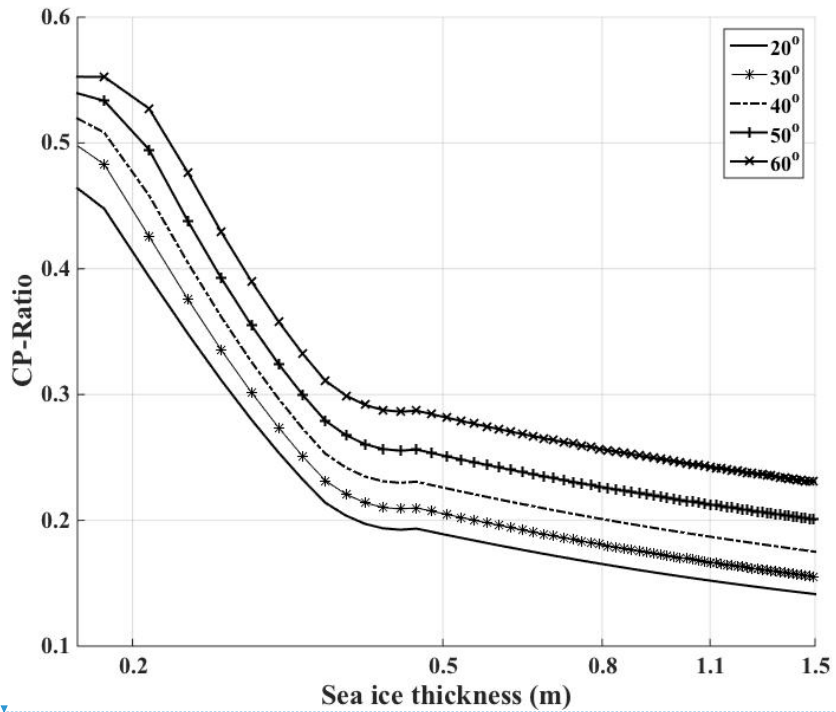


Figure 5. The relationship between *CP-Ratio* and ice thickness at different incidence angles for C-band radar (x-axis in log scale). The incidence angle varies from 20° to 60°. The small-scale roughness parameters are set to $s=0.11$ cm and $l=0.54$ cm (case smooth first-year ice), the standard deviation of the surface slope $\sigma=0.1$.

删除的内容: .

删除的内容: , and the input ice-surface

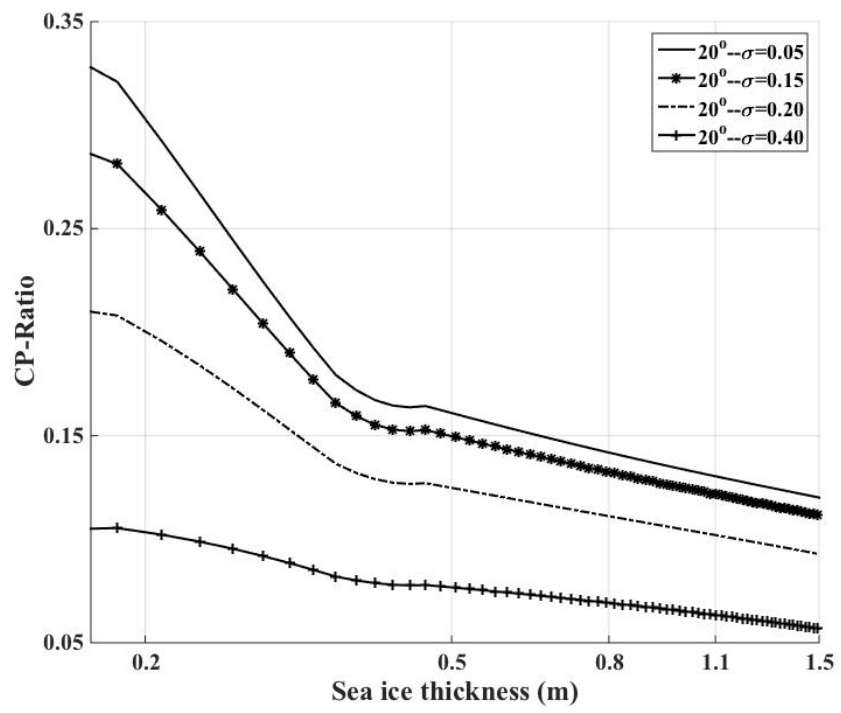
删除的内容: $k_s=$

删除的内容: 15, $kl=2$.

删除的内容: , and

带格式的: 字体:斜体

带格式的: 缩进: 首行缩进: 0 字符



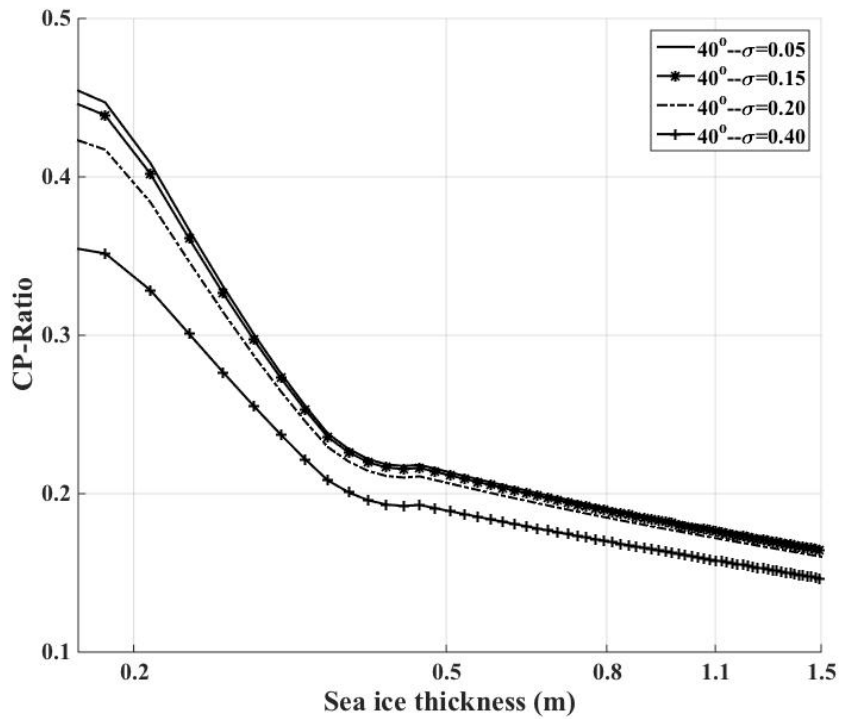


Figure 6. Sensitivity of *CP-Ratio* to the standard deviation of the surface slope σ (x-axis in log scale). The standard deviation of the surface slope σ varies from 0.05 to 0.4, while the small-scale roughness is fixed at $s=0.12$ cm and $l=1.45$ cm (case light nilas). Top figure is for 20° incidence angle and bottom is for 40° incidence angle.

删除的内容: Slope sensitivity for *Ratio*

删除的内容: ks

删除的内容: 15

删除的内容: $kl=2.0$.

删除的内容: 30

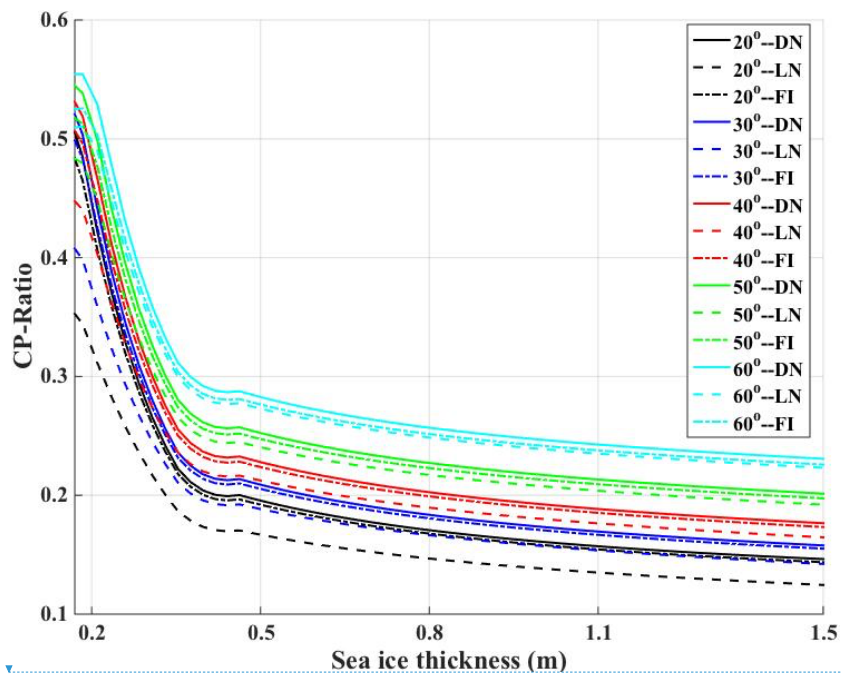


Figure 7. Sensitivity of *CP-Ratio* to the small-scale roughness (x-axis in log scale). The standard deviation of the surface slope σ is fixed at 0.1. Black, blue, red, green and cyan color are for 20°, 30°, 40°, 50°, and 60° incidence angles, respectively. In the legend, DN, LN and FI denote dark nilas, light nilas and smooth first year ice respectively.

删除的内容: .

删除的内容: sensitivity for *Ratio*

带格式的: 字体:非 粗体

删除的内容: Small

删除的内容: RMS height varies from 0.9 mm to 1.8 mm ($k_s=0.1\sim 0.2$), while $k_l=2.0$ and $\sigma=$

删除的内容: color, red color, and

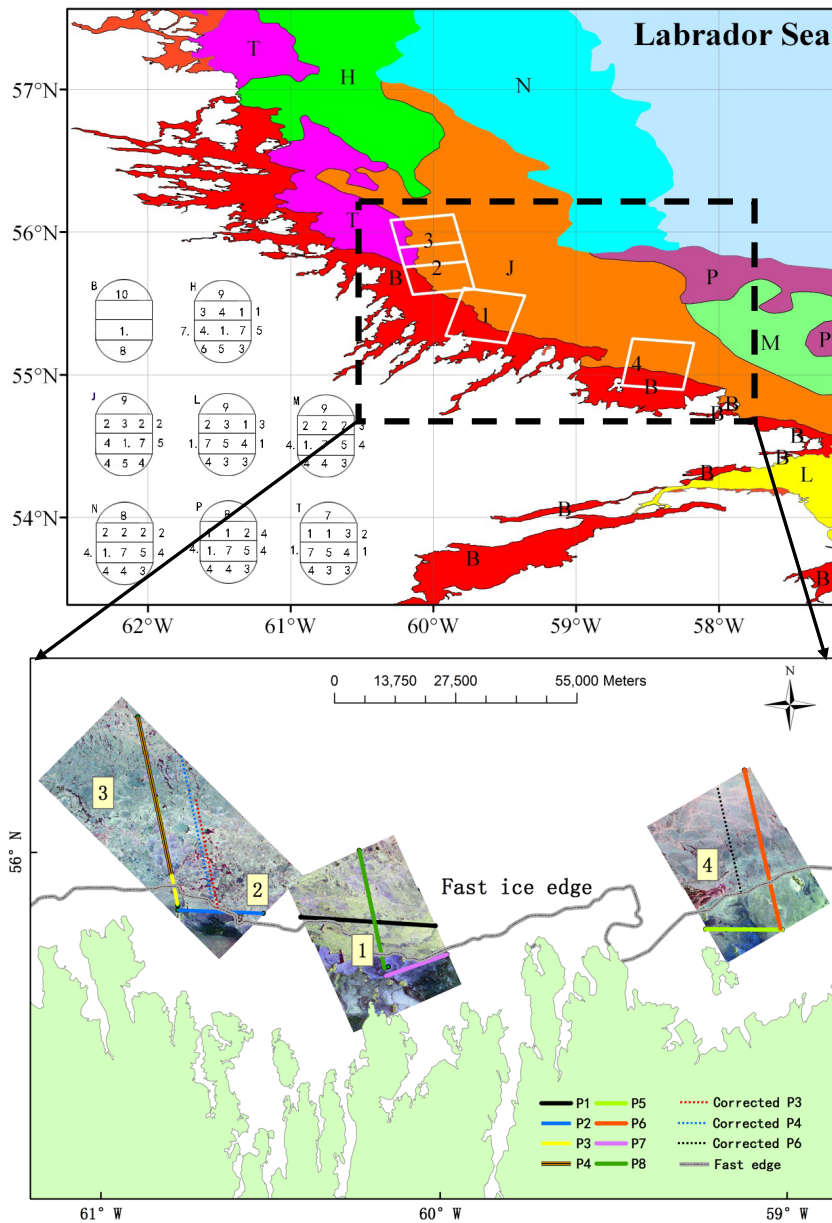
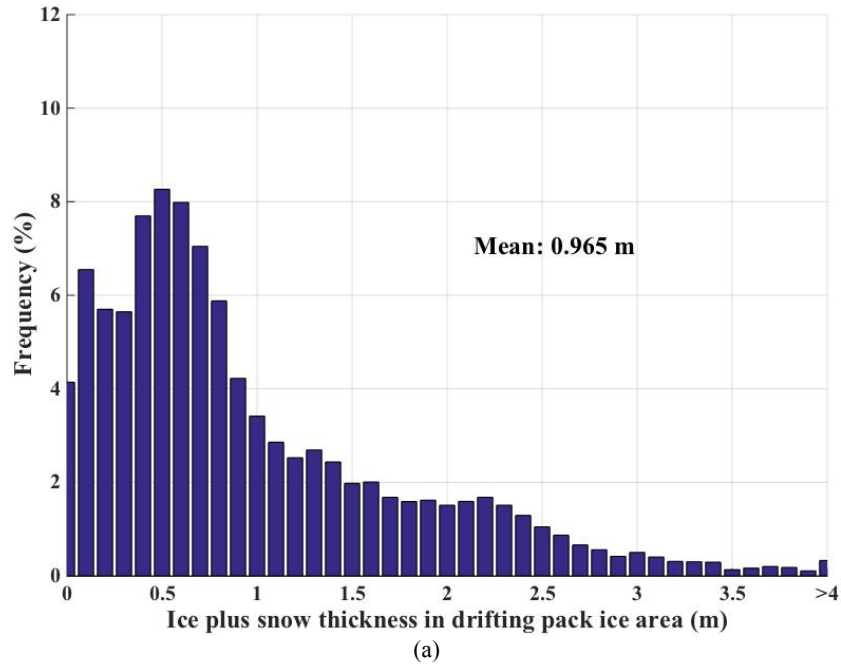


Figure 8. Location of the [study site](#) in the Labrador Sea, with Pauli RGB (HH+VV for blue, HH-VV for red, and HV for green) decompositions of [the RADARSAT-2 images](#).

- 删除的内容: measurement
- 删除的内容: four
- 删除的内容: Radarsat
- 删除的内容: SAR
- 删除的内容: superimposed on the Google Earth© background.

MDA. The specifications of the used SAR data are given in Table 3.

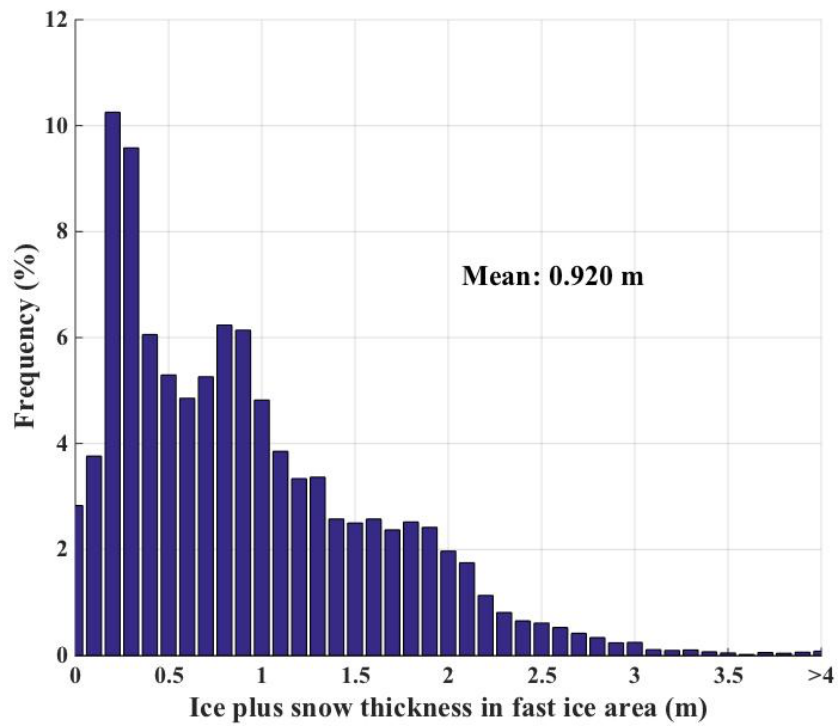


删除的内容: lines overlaid on

删除的内容: the induction sounder flight transects. Red: path-1 (P-1); yellow: path-2 (P-2); green: path-

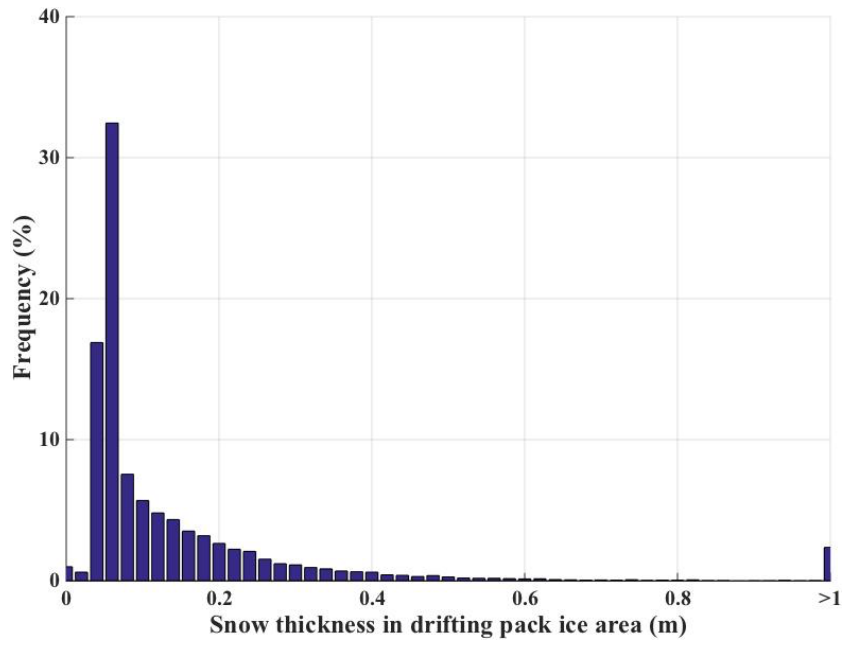
删除的内容: (P-3); cyan: path-4 (P-4); blue: path-5 (P-5); magenta: path-6 (P-6); black: path-7 (P-7); gray: path-8 (P-8).

带格式的: 对齐网格



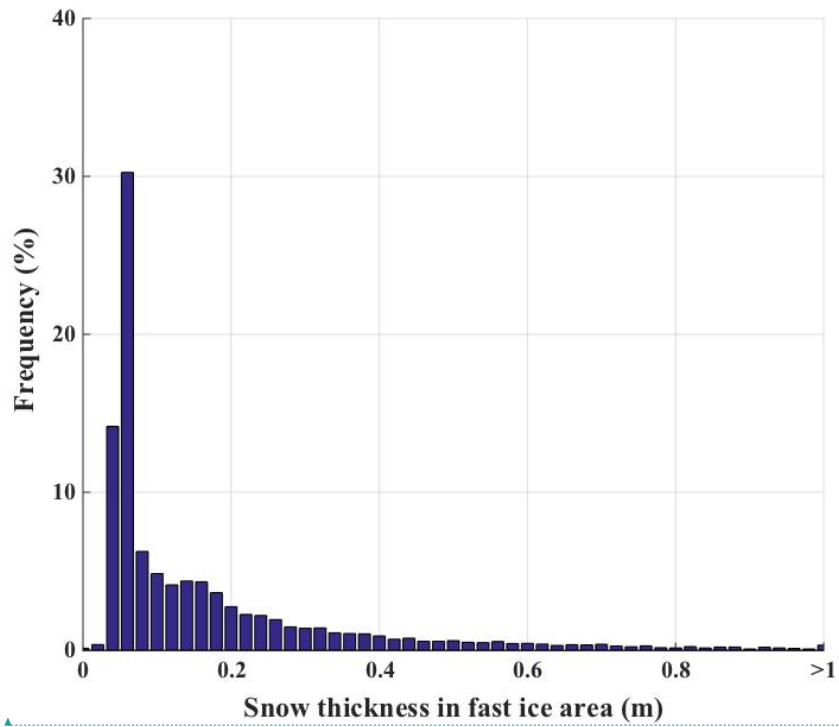
(b)

带格式的: 对齐网格



(c)

带格式的：对齐网格



(d)

Figure 9. Histogram of ice and snow thickness in the Labrador Sea. (a) and (b): Ice plus snow thickness collected with EMS in the pack ice (a) and in the fast ice area (b). (c) and (d): Snow thickness collected with GPR in the pack ice (c) and in the fast ice area (d).

带格式的: 字体:Times New Roman

删除的内容: averaged

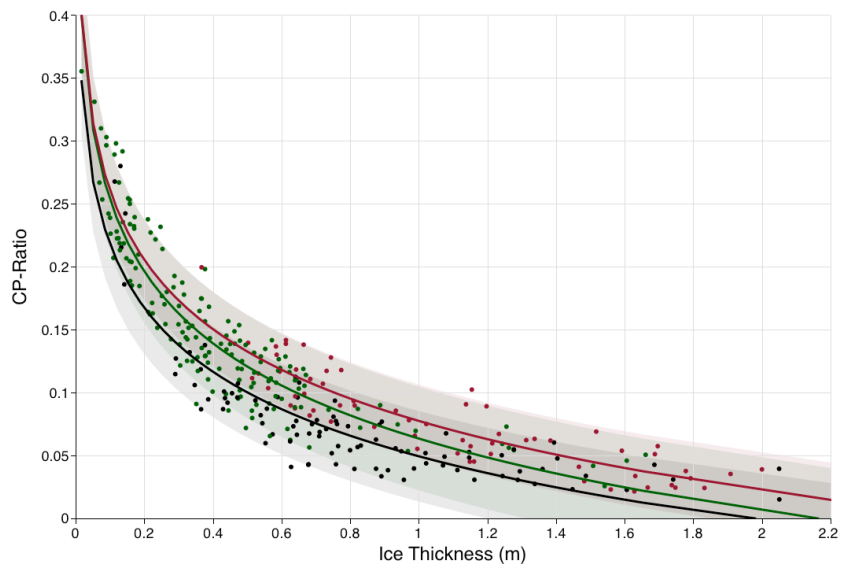
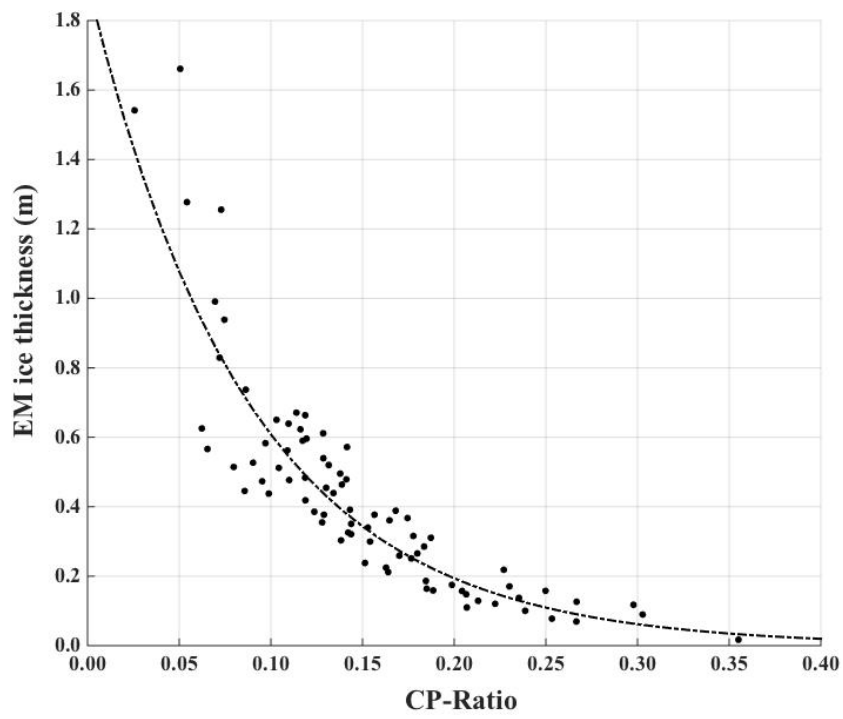


Figure 10. Regressions relating ice thickness to *CP-Ratio* at different incidence angles. The solid lines represent the fits, dashed lines the 90% confidence intervals. The black, green and red colors are used for the incidence angles of 29°, 42° and 49°, respectively.

- 删除的内容: incident angle.
- 删除的内容: solid lines represent the fit, dashed lines the 50% confidence interval. The
- 删除的内容: blue
- 删除的内容: color is
- 删除的内容: angle



(a)

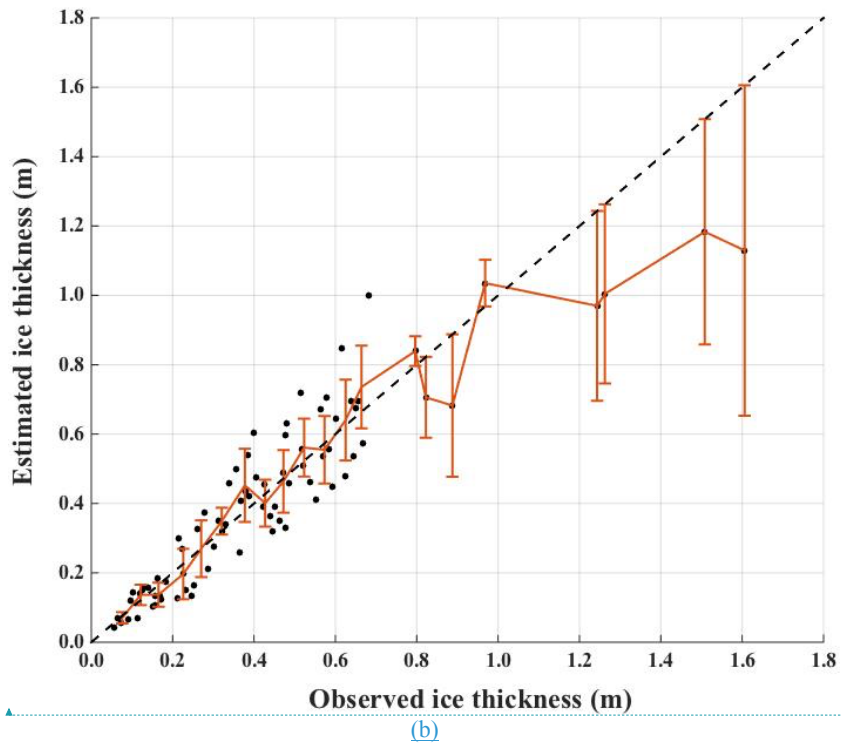


Figure 11. (a) Relationship between the *CP-Ratio* and the observed EM sea thickness. (b) Comparison between the observed and estimated ice thicknesses, and the errorbars show the standard deviation of the plots with respect to the observation data for every 0.05 m segment of ice thickness.

带格式的: 字体:Times New Roman

删除的内容: 12

The second is the dual circular (DC) mode operating a single circular polarization transmission and two orthogonal circular polarizations on reception. The last approach is circular transmission and H and V receptions (called CTLR mode). Among these three compact polarization modes, the latter has been ranked to be the most promising in terms of performance and receiver complexity (Denbina and Collins, 2012; Panigrahi et al., 2012; Salberg et al., 2014). The Mini-SAR on Chandrayaan-1, the first practical radar, is based on the CTLR architecture. The current Indian RISAT-1, the Japanese ALOS-2 and the planned Canadian Radarsat Constellation Mission also support the CTLR mode (Salberg et al., 2014).

In this study, we

Sea ice deformation that results in increased surface roughness is primarily caused by compression processes. Peterson et al. (2008) and Toyota et al. (2009) have shown that the large-scale surface roughness of deformed sea ice is closely linked to the ice thickness due to ridging and rafting. Toyota et al. (2009) indicates that it may be possible to estimate the thickness distribution for deformed ice using roughness properties as proxies. Related to this suggestion, we note that the correlation coefficient between Σ_H and Σ_V could be used as a candidate parameter for determining ice-thickness with large-scale roughness. According to the X-SPM model, the correlation coefficient between Σ_H and Σ_V can be expressed as:

It is only dependent on the standard deviation of the surface slope σ and the incidence angle θ , and independent of the dielectric constant of the sea ice.

Figure 13 shows that the magnitude of the correlation coefficient decreases as σ increases. Further investigation on this issue is needed both theoretically and in comparison to matching field data.

页 55: [3] 删除的内容	张晰	16/3/8 PM4:59:00
-----------------	----	------------------

33, 3531–3541, 2012.

Peterson, I

页 56: [4] 删除的内容	张晰	16/3/8 PM4:59:00
-----------------	----	------------------

Remote, 52, 6521–6533, 2014.

Similä, M., Mäkynen, M., and Heiler, I.: Comparison between C band synthetic aperture radar

页 56: [5] 删除的内容	张晰	16/3/8 PM4:59:00
-----------------	----	------------------

Stiles, W. H, and Ulaby F. T.: The active and passive microwave response to snow parameters, J.

页 59: [6] 删除的内容	张晰	16/3/8 PM4:59:00
-----------------	----	------------------

Resolutions

页 59: [6] 删除的内容	张晰	16/3/8 PM4:59:00
-----------------	----	------------------

Resolutions

页 59: [7] 删除的内容	张晰	16/3/8 PM4:59:00
-----------------	----	------------------

Incident

页 59: [7] 删除的内容	张晰	16/3/8 PM4:59:00
-----------------	----	------------------

Incident

页 59: [8] 删除的内容	张晰	16/3/8 PM4:59:00
-----------------	----	------------------

data

页 59: [8] 删除的内容	张晰	16/3/8 PM4:59:00
-----------------	----	------------------

data